

Depleting inositol pyrophosphate 5-InsP₇ protected the heart against ischaemia–reperfusion injury by elevating plasma adiponectin

Lin Fu ¹, Jimin Du¹, David Furkert², Megan L. Shipton³, Xiaoqi Liu¹, Tim Aguirre², Alfred C. Chin⁴, Andrew M. Riley³, Barry V.L. Potter³, Dorothea Fiedler², Xu Zhang¹, Yi Zhu^{1*}, and Chenglai Fu ^{1,5*}

¹Tianjin Key Laboratory of Metabolic Diseases, Department of Physiology and Pathophysiology, The Province and Ministry Co-sponsored Collaborative Innovation Center for Medical Epigenetics, Tianjin Medical University, 22 Qixiangtai Road, Heping District, Tianjin 300070, China; ²Leibniz-Forschungsinstitut für Molekulare Pharmakologie, Berlin, Germany; ³Medicinal Chemistry and Drug Discovery, Department of Pharmacology, University of Oxford, Mansfield Road, Oxford OX1 3QT, UK; ⁴Weill Cornell/Rockefeller/Sloan Kettering Tri-Institutional MD-PhD Program, New York, NY, USA; and ⁵Institute for Developmental and Regenerative Cardiovascular Medicine, Xinhua Hospital affiliated to Shanghai Jiao Tong University School of Medicine, 1665 Kongjiang Road, Yangpu District, Shanghai 200092, China

Received 14 June 2023; revised 20 November 2023; accepted 30 November 2023; online publish-ahead-of-print 22 January 2024

Time of primary review: 40 days

Aims

Adiponectin is an adipocyte-derived circulating protein that exerts cardiovascular and metabolic protection. Due to the futile degradation of endogenous adiponectin and the challenges of exogenous administration, regulatory mechanisms of adiponectin biosynthesis are of significant pharmacological interest.

Methods and results

Here, we report that 5-diphosphoinositol 1,2,3,4,6-pentakisphosphate (5-InsP₇) generated by inositol hexakisphosphate kinase 1 (IP6K1) governed circulating adiponectin levels via thiol-mediated protein quality control in the secretory pathway. IP6K1 bound to adiponectin and DsbA-L and generated 5-InsP₇ to stabilize adiponectin/ERp44 and DsbA-L/Ero1- α interactions, driving adiponectin intracellular degradation. Depleting 5-InsP₇ by either IP6K1 deletion or pharmacological inhibition blocked intracellular adiponectin degradation. Whole-body and adipocyte-specific deletion of IP6K1 boosted plasma adiponectin levels, especially its high molecular weight forms, and activated AMPK-mediated protection against myocardial ischaemia–reperfusion injury. Pharmacological inhibition of 5-InsP₇ biosynthesis in wild-type but not *adiponectin* knockout mice attenuated myocardial ischaemia–reperfusion injury.

Conclusion

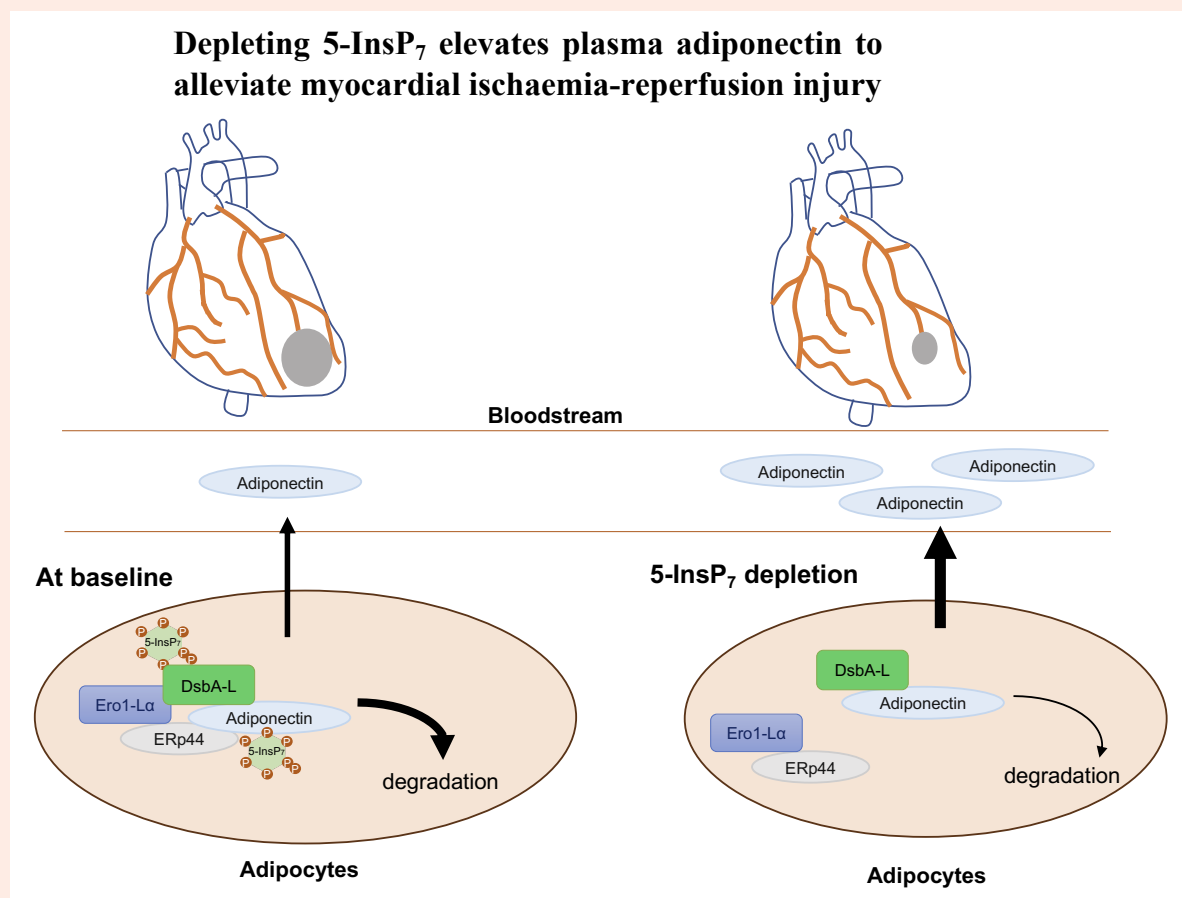
Our findings revealed that 5-InsP₇ is a physiological regulator of adiponectin biosynthesis that is amenable to pharmacological intervention for cardioprotection.

* Corresponding author. Tel: +86 022 8333 6591; Email: zhuyi@tmu.edu.cn (X.Z.); Tel: +86 021 2507 8999; Email: fuchenglai@xinhuaumed.com.cn (C.F.)

© The Author(s) 2024. Published by Oxford University Press on behalf of the European Society of Cardiology.

This is an Open Access article distributed under the terms of the Creative Commons Attribution-NonCommercial License (<https://creativecommons.org/licenses/by-nc/4.0/>), which permits non-commercial re-use, distribution, and reproduction in any medium, provided the original work is properly cited. For commercial re-use, please contact journals.permissions@oup.com

Graphical Abstract



Keywords

IP6K • AMPK • ERp44 • DsbA-L • Ero1-Lα

1. Introduction

Adiponectin is an adipocyte-derived circulating protein with anti-diabetic, anti-inflammatory, and anti-apoptotic properties.¹ Plasma levels of adiponectin are reduced in obese and type 2 diabetic patients.² Lower plasma levels of adiponectin are associated with higher rates of cardiovascular events.³ Replenishing adiponectin has been demonstrated to confer beneficial effects in reducing cardiac ischaemic injury.⁴ The pleiotropic physiological functions of adiponectin are regulated by membrane receptors AdipoR1, AdipoR2, and T-cadherin. Adiponectin binds to its receptors to activate multiple signalling pathways, such as AMPK (AMP-activated protein kinase), p38 MAPK (p38 mitogen-activated protein kinase), PPARα (peroxisome proliferator-activated receptor), and ceramidase.^{5,6} In the bloodstream, adiponectin exists in three major oligomeric forms: trimer, hexamer, and a high molecular weight (HMW) multimer. The latter plays a major role in conferring the protective effects of adiponectin, especially in the cardiovascular system.⁷ These adiponectin complexes are assembled in adipocytes prior to secretion and do not interconvert after secretion.¹

Because the high basal level and rapid elimination rate of adiponectin make exogenous administration challenging,^{8–10} elevating endogenous adiponectin is an alternative approach. Roughly 50% of *de novo*-synthesized adiponectin is retained and degraded intracellularly.¹¹ Thiol-mediated protein quality control in the secretory pathway is orchestrated by

ERp44 (ER protein of 44 kDa), DsbA-L (disulfide-bond A oxidoreductase-like protein), and Ero1-Lα (ER oxidoreductase 1-Lα), which control the intracellular retention of adiponectin^{12–15} and the assembly of HMW adiponectin complexes.^{16,17} However, the mechanisms of coordinating ERp44, DsbA-L, and Ero1-Lα to regulate adiponectin are unclear.

In this study, we identify the intracellular signalling molecule 5-diphosphoinositol 1,2,3,4,6-pentakisphosphate (5-InsP₇) as a critical regulator of endogenous adiponectin levels. 5-InsP₇ levels are increased in obese and type 2 diabetic animal models and contributes to the related disorders.^{18,19} 5-InsP₇ is synthesized from InsP₆ in mammals by a family of three inositol hexakisphosphate kinases (IP6K1, IP6K2, and IP6K3) within specific subcellular areas to mediate diverse cellular processes, including glucose metabolism and protein stability.^{20–22} Functions of individual IP6Ks have been revealed by studies of knockout (KO) mice.²² For example, IP6K1 regulates glucose metabolism; IP6K2 determines cell death; and IP6K3 participates in cytoskeletal remodelling.¹⁸ IP6K1 produces >70% of 5-InsP₇, is the major isoform, and has been proposed to be a therapeutic target for treating metabolic diseases.^{18,21,22} Pharmacological inhibition of 5-InsP₇ biosynthesis demonstrates therapeutic benefit for diabetes,²³ myocardial infarction,²⁴ non-alcoholic fatty liver disease,²⁵ chronic kidney disease,²⁶ etc.²² However, the mechanisms by which depleting 5-InsP₇ attenuates cardiac ischaemia–reperfusion injury have been elusive.

We found that deleting IP6K1 or depleting its product 5-InsP₇ attenuated myocardial ischaemia–reperfusion injury by elevating plasma levels

of adiponectin, especially the HMW form. Pharmacological inhibition of 5-InsP₇ biosynthesis in wild-type (WT) but not *adiponectin* KO mice alleviated myocardial ischaemia–reperfusion injury. IP6K1, via its enzymatic product 5-InsP₇, drove intracellular retention and degradation of adiponectin by strengthening adiponectin/ERp44 and DsbA-L/Ero1-L α complex formation. Our findings reveal a novel molecular mechanism governing adiponectin biosynthesis that is pharmacologically targetable.

2. Methods

2.1 Cell culture and transfection

Human embryonic kidney (HEK) 293 cells and 3T3-L1 pre-adipocytes were purchased from ATCC (American Type Culture Collection). WT mouse embryonic fibroblast (MEF) cells and IP6K1 KO MEF cells were isolated as previous report and cultured in DMEM medium (Thermo Fisher Scientific) supplemented with 10% (v/v) FBS (Thermo Fisher Scientific), 100 U/mL penicillin, and 100 μ g/mL streptomycin (Thermo Fisher Scientific). All cells were maintained at 37°C with 5% CO₂. Before treating cells, the existing cell culture medium was exchanged with fresh medium. Transfections were conducted with Lipofectamine 3000 (Thermo Fisher Scientific). Cycloheximide (#2112) was purchased from Cell Signaling Technology. Chloroquine (C6628) and N²-(*m*-(trifluoromethyl)benzyl) N⁶-(*p*-nitrobenzyl)purine (TNP cat. no. T3955), an inhibitor of IP6K, were purchased from Millipore Sigma. MG132 (S2619) was purchased from Selleck Chemicals.

2.2 Animal experiments

WT and IP6K1 KO mice were littermates from heterozygous breeding. Adipocyte-specific IP6K1 KO mice (*adipoq*-cre; IP6K1^{fl/fl}) were generated by crossing *adipoq*-cre strain with IP6K1^{fllox/fllox} (IP6K1^{fl/fl}). Cardiomyocyte-specific IP6K1 KO mice (*α MyHC*-cre; IP6K1^{fl/fl}) were generated by crossing *α MyHC*-cre strain with IP6K1^{fl/fl}. *Adiponectin* KO mice were obtained from The Jackson Laboratory.

Mouse myocardial ischaemia–reperfusion injury: Male mice aged 8–12 weeks were anaesthetized by using 2% isoflurane and placed in a supine position on a heating pad (37°C), followed by a left thoracotomy between the third and fourth ribs to expose the heart. The left anterior descending coronary artery was ligated by using a 7-0 Prolene suture. The occlusion was removed after 30 min to allow myocardial reperfusion for 24 h.

Evans blue and 2,3,5-triphenyltetrazolium chloride (TTC) staining: Mice were anaesthetized by using 1.2% 2,2,2-tribromoethanol (TBE; Cas:75-80-9, Aladdin) in order to produce less bradycardia with less effect on cardiac loading and ventricular function than does xylazine–ketamine,²⁷ then injected with 0.5% (w/v) Evans blue (AAA1677409, Thermo Fisher Scientific) via jugular vein after occlusion of left anterior descending coronary artery. The animal was euthanized, and the heart was then excised, washed with PBS, and frozen at –20°C for 20 min. The heart was cut transversely into 2 mm thin slices and was incubated with 2% (w/v) solution of TTC (AAA1087009, Thermo Fisher Scientific) in PBS buffer (pH 7.4 at 37°C) for 20 min. The heart slices were then fixed for 30 min in 4% (w/v) paraformaldehyde. The non-ischaemic portion was stained blue, viable tissue within the region at risk was stained bright red, and infarcted tissue was white. The images were analysed using ImageJ, and the infarct size ratio was calculated by dividing the infarct volume to the left ventricle volume, and infarct volume to the area at risk.

Echocardiography: Mice were anaesthetized with 2% isoflurane and placed in a supine position on a heating pad (37°C). Echocardiogram was performed by using a Vevo 2100 system and MS-400 linear probe. A short-axis view of the left ventricle at the level of the papillary muscles was obtained, and M-mode recordings were obtained from this view. Fractional shortening and ejection fraction were calculated or measured from M-mode echocardiography.

TNP was dissolved in DMSO:Tween 80:water (1:1:8) and was injected intraperitoneally (20 mg/kg; body weight) for 1 week. Blood was collected by cardiac puncture. Ischaemia–reperfusion injury was performed after

TNP treatment, and animals were sacrificed 24 h later. Evans blue and TTC staining was performed to analyse the infarction area.

All animal-related procedures were conducted in accordance with the NIH Guide for Care and Use of Laboratory Animals and approved by the Animal Care and Use Committee of Tianjin Medical University. The approval number for animal experiments is TMUaMEC 2019005.

2.3 TUNEL staining assay

Animals were euthanized by CO₂, perfused with PBS, and fixed with 4% (w/v) paraformaldehyde. Hearts were excised and incubated in 4% (w/v) paraformaldehyde for at least 48 h. TUNEL staining was performed on heart sections according to the manufacturer's suggestions (One-step TUNEL Apoptosis Assay Kit, Abbkine Scientific). The nucleus was counter-stained with diamidino-2-phenylindole (DAPI). Cardiomyocytes were stained by utilizing anti-cardiac troponin I antibodies (66376-1-Ig, Proteintech). Pictures were recorded by using a confocal microscope (Zeiss LSM 800).

2.4 Isolate and culture of primary adipocytes

Male C57BL/6 mice (8–9 weeks of age) were euthanized by CO₂. The subcutaneous fat pads were harvested, washed in PBS (pH 7.4) buffer at room temperature, and minced thoroughly (2–3 mm in diameter) in collagenase solution (0.2 mg/mL collagenase I). This mixture was incubated at 37°C with shaking at 220 rpm for 1 h. After digestion, the mixture was filtered through a 70 μ m mesh into a 50 mL conical polypropylene tube and allowed to stand for 2–3 min. The floating layer of adipocytes was collected and washed three times. The cells were incubated in alpha modified Eagle's medium containing 20% foetal bovine serum.

2.5 Western blotting and immunoprecipitation

Tissues and cells were homogenized at 4°C in lysis buffer containing 50 mM Tris-HCl (pH 7.4), 100 mM NaCl, 0.5% Igepal CA630, 5 mM MgCl₂, and protease/phosphatase inhibitors (Millipore Sigma). Lysates were pulse sonicated and centrifuged at 13 000 g for 10 min at 4°C. The supernatants were collected. Protein concentrations were determined using a Pierce BCA Protein Assay Kit (Thermo Fisher Scientific). SDS loading buffer (Solaribo) containing 5% β -mercaptoethanol was added, and the samples were boiled for 5 min.

For immunoprecipitation, tissues and cells were homogenized at 4°C in the aforementioned lysis buffer. Lysates were passed through 30-gauge needles 20 times and centrifuged at 13 000 g for 10 min at 4°C. The supernatants were collected and pre-cleaned with protein A/G beads (Santa Cruz) for 90 min at 4°C. Lysates were centrifuged briefly, and the supernatants were collected while the protein A/G beads were discarded. Primary antibody was added to cell lysates and incubated at 4°C overnight. Protein A/G beads were then added to the cell lysates and incubated for 2 h at 4°C. The beads were washed with cold lysis buffer three times. 1.5 \times SDS loading buffer containing 5% β -mercaptoethanol was added, and the samples were boiled for 5 min.

Samples were run on 10% polyacrylamide gels and transferred to nitrocellulose membranes (Thermo Fisher Scientific). Membranes were blocked with 5% non-fat milk in TBST, or 5% bovine serum albumin (BSA; Thermo Fisher Scientific) in TBST for phospho-antibodies, for 30 min at room temperature, washed with TBST, and incubated with primary antibodies in 5% BSA in TBST overnight at 4°C. The following day, membranes were washed with TBST, incubated with secondary antibodies for 1 h at room temperature, and washed again with TBST. Chemiluminescent substrate (Thermo Fisher Scientific) was used to visualize protein bands.

Antibodies against IP6K1 (sc-374292), IP6K2 (sc-373770), myc-tag (clone 9E10), ERp44 (sc-393687), Ero1-L α (sc-365526), T-cadherin (sc-166875), adipoR2 (sc-514045), and GRP78 (sc-166490) were purchased from Santa Cruz Biotechnology. Antibodies against adiponectin (ab22554) and adipoR1 (ab70362) were purchased from Abcam. Antibodies against β -actin (66009-1-Ig), cardiac troponin I (66376-1-Ig), and DsbA-L (GSTK1

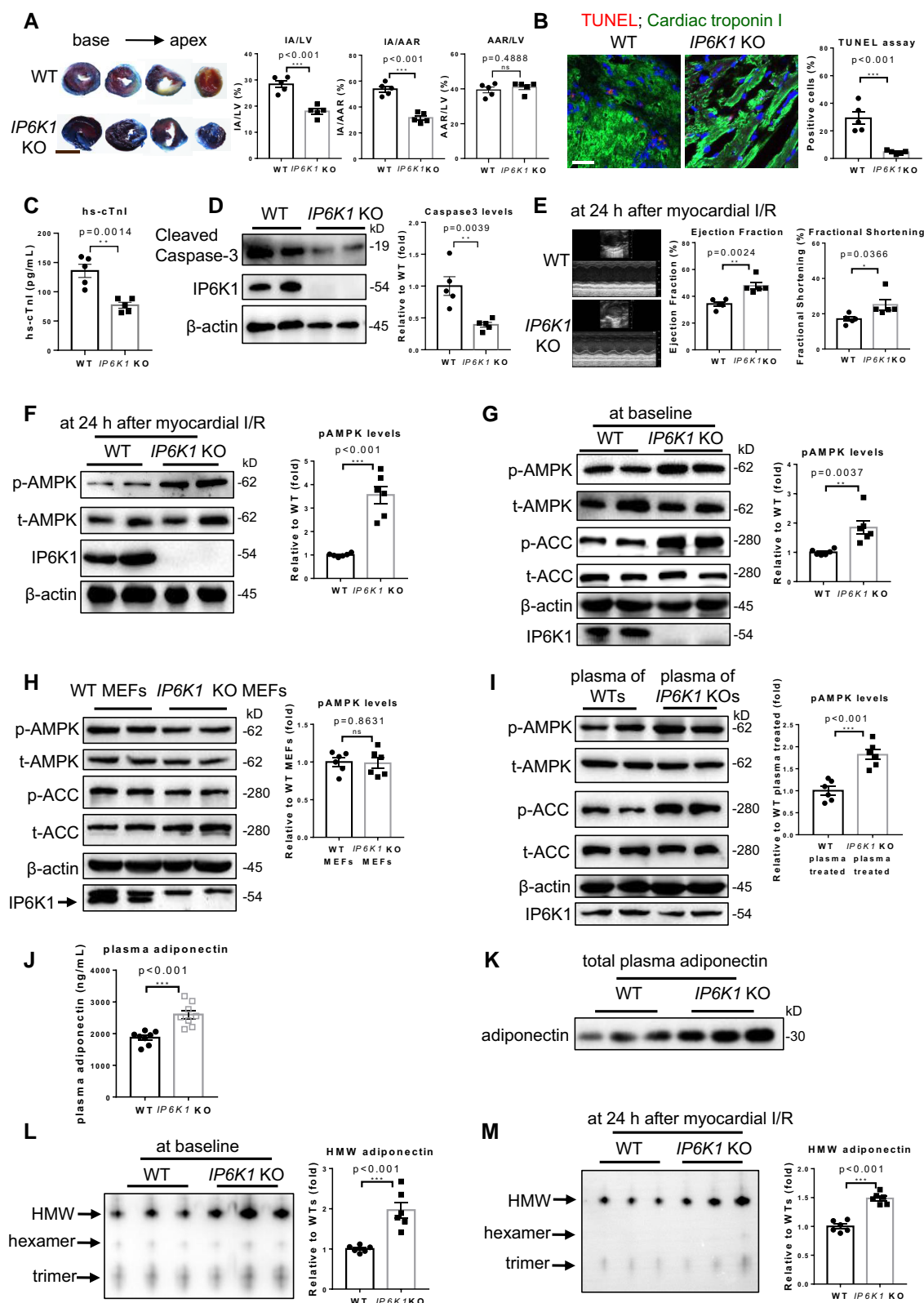


Figure 1 Knocking out IP6K1 attenuated myocardial ischaemia-reperfusion injury. (A) Evans blue and TTC double staining of the hearts at 24 h after myocardial ischaemia-reperfusion injury. The non-ischaemic area was indicated by blue, the area at risk (AAR) by red and white, and the infarct area (IA) by white. LV, left ventricle. Data were presented as mean \pm SEM, ns = not significant, Student's *t*-test, *n* = 5 mice per group. Scale bar: 5 mm. (B) TUNEL staining of the ischaemia-reperfusion injured hearts in the border zones. Cardiac troponin I was co-stained for cardiomyocytes. Data were presented as mean \pm SEM, Student's *t*-test, *n* = 5 mice per group. Scale bar: 20 μ m. (C) Plasma levels of hs-cTn-I at 24 h after myocardial ischaemia-reperfusion injury. Data were presented as mean \pm SEM, Student's *t*-test, *n* = 5 mice per group. (D) Protein levels of cleaved caspase 3 in the border zones of ischaemia-reperfusion injured (continued)

Figure 1 Continued

hearts. Data were presented as mean \pm SEM, Student's *t*-test, *n* = 5 mice per group. (E) Representative echocardiographic images of WT and *IP6K1* KO mice at 24 h after the myocardial ischaemia–reperfusion injury. Data were presented as mean \pm SEM, Student's *t*-test, *n* = 5 mice per group. (F) Phosphorylation levels of AMPK in the border zones of the ischaemic hearts. Data were presented as mean \pm SEM, Student's *t*-test, *n* = 6 mice per group. (G) Phosphorylation levels of AMPK in WT and *IP6K1* KO hearts at baseline. Data were presented as mean \pm SEM, Student's *t*-test, *n* = 6 mice per group. (H) Phosphorylation levels of AMPK in cultured WT and *IP6K1* KO MEF cells. Data were presented as mean \pm SEM, ns = not significant, Student's *t*-test, *n* = 6 from three independent repeats. (I) Phosphorylation levels of AMPK in WT MEFs that were treated with plasma from WT or *IP6K1* KO mice. Data were presented as mean \pm SEM, Student's *t*-test, *n* = 6 mice per group. (J) Plasma adiponectin concentrations that were determined by ELISA. Data were presented as mean \pm SEM, Student's *t*-test, *n* = 8 mice per group. (K) Total circulating adiponectin levels in WT and *IP6K1* KO mice, *n* = 3 mice per group. (L) Adiponectin oligomers in the plasma of WT and *IP6K1* KO mice. Data were presented as mean \pm SEM, Student's *t*-test, *n* = 6 mice per group. (M) Adiponectin oligomers in the plasma of WT and *IP6K1* KO mice at 24 h after the myocardial ischaemia–reperfusion injury. Data were presented as mean \pm SEM, Student's *t*-test, *n* = 6 mice per group.

cat. no. 14535-1-AP) were purchased from Proteintech. Antibodies against AMPK (9158s), phospho-AMPK α (Thr172; 2535s), ubiquitin (3936s), cleaved caspase 3 (9664s), acetyl-CoA carboxylase (3676s), and phospho-acetyl-CoA carboxylase (Ser79; 11818s) were purchased from Cell Signaling Technology. Antibody against IP6K3 (PA5-106525) was purchased from Thermo Fisher Scientific. Antibody against IP6K1 (HPA040825) and flag-tag (MAB3118) was purchased from Millipore Sigma.

2.6 Enzyme-linked immunosorbent assay

Animals were euthanized by CO₂. Blood samples were collected via cardiac puncture. The plasma concentrations of adiponectin were determined by using a Mouse Adiponectin ELISA Kit, following the manufacturer's instructions (PA002, Beyotime). The plasma levels of high-sensitivity cardiac troponin I (hs-cTn-I) were determined by using a mouse hs-cTn-I ELISA Kit, following the manufacturer's instructions (BY-EM222975, BYabscience).

2.7 Western blot analyses of plasma adiponectin oligomerization

Plasma samples were mixed with buffer containing 62.5 mM Tris-HCl (pH 6.8), 10% glycerol, and 0.01% bromophenol blue. Samples were separated by the native polyacrylamide gel electrophoresis. Proteins were then transferred to a PVDF membrane. Primary antibody against adiponectin was used to detect the oligomers of adiponectin.

2.8 Immunofluorescence staining

Cultured cells were washed with PBS and fixed with 4% (w/v) paraformaldehyde for 10 min. The samples were blocked with 10% (v/v) goat serum (MilliporeSigma) for 10 min at room temperature and then incubated with primary antibodies at 4°C overnight. The samples were washed multiple times with PBS for 3 h at room temperature and then incubated with fluorescent-dye conjugated secondary antibodies for 1 h at room temperature. Nuclei were stained with DAPI (Thermo Fisher Scientific) for 10 min. Slices were mounted with ProLong Gold Antifade Mountant (Thermo Fisher Scientific). Pictures were taken under a confocal microscope (Zeiss LSM 800). Alexa Fluor 568 Goat Anti-Rabbit and Alexa Fluor 488 Goat Anti-Mouse secondary antibodies were purchased from Thermo Fisher Scientific.

2.9 RNA isolation and real-time PCR

Total RNA was isolated from mice tissues using the TransZol up Plus RNA Kit (TransGen Biotech) and was reverse transcribed to cDNA using SuperScript® III (Invitrogen) according to the manufacturer's recommended protocol. Real-time quantitative PCR was performed with the Brilliant II SYBR Green qPCR Master Mix (Stratagene) and the ABI 7900HT Real-time PCR System (Life Technologies). β -Actin was used as loading control.

2.10 Plasmid cloning

Myc-tagged IP6K1, myc-tagged GFP, flag-tagged GFP, flag-tagged adiponectin, flag-tagged DsbA-L, flag-tagged ERp44, flag-tagged Ero1- α , GST-fused

ERp44, and GST-fused DsbA-L were cloned into the pCDH-EF1-MCS-T2A-copGFP vector (System Biosciences). The PCR products were generated by using Prime Star DNA Polymerase (Takara Bio) and inserted into the vectors using the In-Fusion HD Enzyme (Takara Bio). All newly constructed plasmids were sequence verified.

2.11 Subcellular fractionations

Isolation of the endoplasmic reticulum (ER) was performed by using an ER isolation kit (Sigma-Aldrich, ER0100) according to the manufacturer's instructions.

2.12 Chemical synthesis

5-PCF₂Am-InsP₅ (CF2) and 5-PCP-InsP₅ (5PCP) were synthesized as previously described.^{28,29} The inositol pyrophosphates 1-diphosphoinositol pentakisphosphate (1-InsP₇), 3-diphosphoinositol pentakisphosphate (3-InsP₇), and 5-InsP₇ were synthesized using similar methods to those previously described.³⁰ All synthetic compounds were purified by ion-exchange chromatography, fully characterized by ¹H, ³¹P, and ¹³C NMR spectroscopy and where feasible quantified by total phosphate analysis. Commercially available InsP₆ (MilliporeSigma) was utilized. 1/3-position 5PCP-resin was synthesized as previously described.³¹ SC-919 was synthesized as previously described.²⁶

2.13 In vitro protein binding assay

To assess the binding of adiponectin with ERp44, flag-tagged adiponectin and GST-fused ERp44 were overexpressed in HEK293 cells. Cell lysates were pre-cleaned with protein A/G beads (Santa Cruz Biotechnology), and anti-flag-tag antibody was added to cell lysates expressing flag-tagged adiponectin overnight. Flag-tagged adiponectin was pulled down by protein A/G beads and washed three times. Separately, Glutathione Sepharose (GE Life Sciences) was used to pull down GST-fused ERp44, and PreScission Protease (Beyotime Biotechnology) was applied to cleave GST and release ERp44 into the buffer. Buffer with purified ERp44 was added to protein A/G agarose-bound flag-tagged adiponectin in the presence of InsP₆, 5-InsP₇, 5PCP, CF2, 1-InsP₇, 3-InsP₇, InsP₃, InsP₄, or InsP₅ overnight at 4°C. The beads were then collected and washed three times. The samples were loaded with 1.5 \times SDS loading buffer containing 5% β -mercaptoethanol and boiled for 5 min. The *in vitro* binding of DsbA-L with Ero1- α was performed by utilizing flag-tagged Ero1- α and GST-fused DsbA-L, which were produced in HEK293 cells. Purified DsbA-L was added to protein A/G agarose-bound flag-tagged Ero1- α in the presence of InsP₆, 5-InsP₇, 5PCP, CF2, 1-InsP₇, 3-InsP₇, InsP₃, InsP₄, or InsP₅ overnight at 4°C. The beads were then collected and washed three times. The samples were loaded with 1.5 \times SDS loading buffer containing 5% β -mercaptoethanol and boiled for 5 min.

To assess the binding of adiponectin to 5PCP, the control and 5PCP-resin were equilibrated with cell lysis buffer. Adiponectin, prepared from GST-fused adiponectin via Glutathione Sepharose and PreScission Protease, was added onto the 5PCP-resin and incubated overnight at 4°C. The resins were collected and washed three times. The samples were mixed with 1.5 \times SDS loading buffer containing 5% β -mercaptoethanol

and boiled for 5 min. The binding of DsbA-L to 5PCP was performed by the same method. DsbA-L was prepared from GST-fuse DsbA-L via Glutathione Sepharose and PreScission Protease.

D-myo-inositol-1,4,5-triphosphate (InsP₃, cat. no. 10008205), D-myo-inositol-1,3,4,5-tetrakisphosphate (InsP₄, cat. no. 60980), and D-myo-inositol-1,3,4,5,6-pentakisphosphate (InsP₅, cat. no. 10007784) were purchased from Cayman Chemical. D-myo-inositol-1,2,3,4,5,6-hexakisphosphate (InsP₆, cat#P8810) was purchased from MilliporeSigma.

2.14 Statistical analysis

All statistical data were presented as means \pm SEM. Experiments were repeated at least three times for the quantifications. Unpaired two-tailed Student's *t*-test was used to test for significance when comparing two groups. One-way ANOVA was used for comparison of more than two groups, and the adjusted *P* value was determined by Dunnett's multiple comparisons test. ImageJ was used to analyse western blots. Volocity software (V6.3, PerkinElmer Inc.) was used to quantify the co-localization. Differences were considered significant at **P* < 0.05, ***P* < 0.01, and ****P* < 0.001. GraphPad Prism 7.0 was used for all statistical analyses.

3. Results

3.1 Knocking out IP6K1 protected the heart from myocardial ischaemia–reperfusion injury

We utilized IP6K1 KO mice to study the role of IP6K1 in myocardial ischaemia–reperfusion injury. Animals were subjected to 30 min ischaemia followed by 24 h reperfusion; the myocardial infarction was analysed by Evans blue/TTC staining (Figure 1A). Compared to WT littermates, the size of the infarct area was smaller in the IP6K1 KO mice (Figure 1A). At the cellular level, there were fewer apoptotic cardiomyocytes in the border zone of IP6K1 KO hearts than in WT littermates after ischaemia–reperfusion injury (Figure 1B). The plasma levels of hs-cTn-I, a marker for cardiomyocyte damage, were lower in the IP6K1 KO mice than WT littermates after ischaemia–reperfusion injury (Figure 1C). We performed western blots to check the levels of cleaved caspase 3, a marker for apoptosis, in the border zone. Its levels were lower in the IP6K1 KO preparations than WT littermates (Figure 1D). Cardiac functions revealed by echocardiogram showed that the ejection fraction and fractional shortening were similar in WT and IP6K1 KO littermates at baseline (see Supplementary material online, Figure S1), but were higher in IP6K1 KO mice than those of WT littermates after ischaemia–reperfusion injury (Figure 1E). These results suggested that deletion of IP6K1 protected the heart from myocardial ischaemia–reperfusion injury.

The AMPK signalling pathway has been shown to protect against myocardial ischaemia–reperfusion injury.³² Western blots showed that the levels of phospho-AMPK were higher in the IP6K1 KO hearts than those of WT littermates at both ischaemic and non-ischaemic conditions (Figure 1F and G), suggesting that activation of the AMPK signalling may contribute to the attenuated ischaemia–reperfusion injury observed in IP6K1 KO mice. We utilized *in vitro* cultured MEF cells to validate whether deletion of IP6K1 directly increases AMPK phosphorylation in the same cell system (Figure 1H). However, we did not observe activation of the AMPK pathway in IP6K1 KO MEFs in the *in vitro* cell culture (Figure 1H), which is consistent with a recent finding that depletion of 5-InsP₇ does not itself activate the AMPK pathway in HCT116 cells.³³ This puzzle prompted us to check the animal plasma to establish whether deletion of IP6K1 might augment certain factors to activate the AMPK pathway. Cells were treated with plasma from WT and IP6K1 KO littermates. The levels of phospho-AMPK were elevated when cells were treated with plasma from IP6K1 KO mice (Figure 1I). Adiponectin has been shown to activate the AMPK pathway to protect against myocardial ischaemia–reperfusion injury.⁴ We found that the plasma levels of adiponectin were higher in IP6K1 KO animals (Figure 1J). Western blots confirmed that the plasma levels of both the total and HMW adiponectin were elevated in IP6K1 KO mice (Figure 1K and L). The expression levels of adiponectin receptors

AdipoR1, AdipoR2, and T-cadherin were equal between WT and IP6K1 KO littermates (see Supplementary material online, Figure S2), suggesting that the activated AMPK signalling in IP6K1 KO mice was not through upregulation of adiponectin receptors. The plasma HMW adiponectin levels were still higher in IP6K1 KO mice after ischaemia–reperfusion injury (Figure 1M).

3.2 Adipocyte-specific deletion of IP6K1 attenuated myocardial ischaemia–reperfusion injury

To confirm the *in vivo* effects of IP6K1 deletion upon adiponectin, we generated adipocyte-specific IP6K1 KO mice (*adipoq-cre; IP6K1^{fl/fl}*). Similar to the effects of whole-body KO of IP6K1, adipocyte-specific deletion of IP6K1 (*adipoq-cre; IP6K1^{fl/fl}*) boosted the plasma levels of adiponectin (Figure 2A). Consistently, the HMW forms of plasma adiponectin were higher in the adipocyte-specific IP6K1 KO mice (*adipoq-cre; IP6K1^{fl/fl}*) than those of control animals (IP6K1^{fl/fl}; Figure 2B). The elevated plasma levels of adiponectin in adipocyte-specific IP6K1 KO mice also activated the AMPK pathway in the heart (Figure 2C).

We utilized the adipocyte-specific IP6K1 KO mice (*adipoq-cre; IP6K1^{fl/fl}*) to explore the protective effect of the elevated adiponectin against cardiac ischaemia–reperfusion injury. After the ischaemia–reperfusion injury, the adipocyte-specific IP6K1 KO mice (*adipoq-cre; IP6K1^{fl/fl}*) showed lower plasma levels of the cardiomyocyte damage marker hs-cTn-I than the controls (IP6K1^{fl/fl}; Figure 2D). The size of infarct area was smaller in the adipocyte-specific IP6K1 KO mice (*adipoq-cre; IP6K1^{fl/fl}*) than those of controls (IP6K1^{fl/fl}; Figure 2E). The echocardiogram revealed that the adipocyte-specific IP6K1 KO mice (*adipoq-cre; IP6K1^{fl/fl}*) had higher ejection fraction and fractional shortening than the controls (IP6K1^{fl/fl}) after ischaemia–reperfusion injury (Figure 2F). The levels of phospho-AMPK were higher in the border zone of ischaemia–reperfusion injured hearts of adipocyte-specific IP6K1 KO mice (*adipoq-cre; IP6K1^{fl/fl}*) compared to controls (IP6K1^{fl/fl}; Figure 2G), whereas the expression levels of the cleaved caspase 3 were lower in the border zone of ischaemia–reperfusion injured hearts in adipocyte-specific IP6K1 KO mice (*adipoq-cre; IP6K1^{fl/fl}*) compared to controls (IP6K1^{fl/fl}; Figure 2H). Thus, deletion of IP6K1 in adipocytes elevated circulating adiponectin levels and alleviated myocardial ischaemia–reperfusion injury.

3.3 Cardiomyocyte-specific deletion of IP6K1 did not elevate adiponectin and did not attenuate myocardial ischaemia–reperfusion injury

Cardiomyocytes also express adiponectin, which attenuates ischaemia–reperfusion injury in an autocrine manner.³⁴ To examine whether deletion of IP6K1 could also elevate cardiomyocyte-derived adiponectin to protect the ischaemic heart, we generated cardiac-specific IP6K1 KO mice (*αMyHC-cre; IP6K1^{fl/fl}*). Deletion of IP6K1 in cardiomyocytes did not affect the adiponectin protein levels in the heart (see Supplementary material online, Figure S3A). The plasma levels of adiponectin were similar between control (IP6K1^{fl/fl}) and cardiac-specific IP6K1 KO (*αMyHC-cre; IP6K1^{fl/fl}*) mice (see Supplementary material online, Figure S3B). The phosphorylation levels of AMPK in the heart were similar between control (IP6K1^{fl/fl}) and cardiac-specific IP6K1 KO (*αMyHC-cre; IP6K1^{fl/fl}*) mice at baseline (see Supplementary material online, Figure S3C).

We examined whether specific deletion of IP6K1 in cardiomyocytes could attenuate cardiac ischaemia–reperfusion injury (see Supplementary material online, Figure S3D and E). The results showed that the AMPK pathway in the ischaemia–reperfusion injured heart was not activated in the cardiac-specific IP6K1 KO (*αMyHC-cre; IP6K1^{fl/fl}*) mice (see Supplementary material online, Figure S3D). The infarct sizes were similar between control (IP6K1^{fl/fl}) and cardiac-specific IP6K1 KO (*αMyHC-cre; IP6K1^{fl/fl}*) mice (see Supplementary material online, Figure S3E). Thus, cardiomyocyte-specific deletion of IP6K1 did not elevate adiponectin and did not attenuate myocardial ischaemia–reperfusion injury.

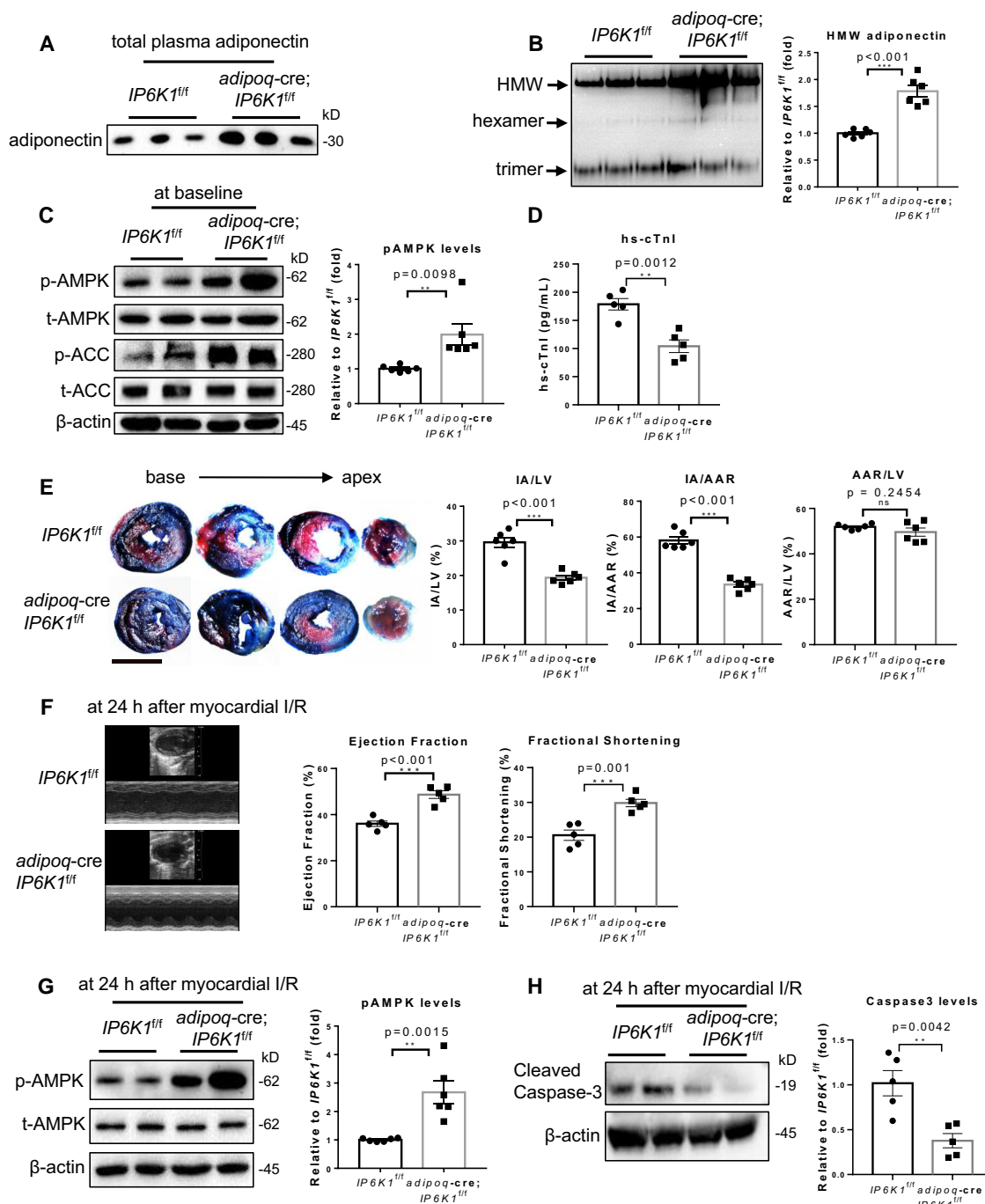


Figure 2 Adipocyte-specific deletion of IP6K1 attenuated myocardial ischaemia-reperfusion injury. (A) Total circulating adiponectin levels in control (*IP6K1^{fl/fl}*) and adipocyte-specific *IP6K1* KO mice (*adipoq-cre; IP6K1^{fl/fl}*). $n = 3$ mice per group. (B) Levels of plasma adiponectin oligomers in control and adipocyte-specific *IP6K1* KO mice. Data were presented as mean \pm SEM, Student's *t*-test, $n = 6$ mice per group. (C) Phosphorylation levels of AMPK in heart tissues of control and adipocyte-specific *IP6K1* KO mice. Data were presented as mean \pm SEM, Student's *t*-test, $n = 6$ mice per group. (D) Plasma levels of hs-cTn-I at 24 h after myocardial ischaemia-reperfusion injury in control and adipocyte-specific *IP6K1* KO mice. Data were presented as mean \pm SEM, Student's *t*-test, $n = 5$ mice per group. (E) Evans blue and TTC double staining of the hearts in control and adipocyte-specific *IP6K1* KO mice at 24 h after myocardial ischaemia-reperfusion injury. The non-ischaemic area was indicated by blue, the area at risk (AAR) by red and white, and the infarct area (IA) by white. LV, left ventricle. Data were presented as mean \pm SEM, Student's *t*-test, $n = 6$ mice per group. Scale bar: 5 mm. (F) Representative echocardiographic images of control and adipocyte-specific *IP6K1* KO mice at 24 h after myocardial ischaemia-reperfusion injury. Data were presented as mean \pm SEM, Student's *t*-test, $n = 5$ mice per group. (G) Phosphorylation levels of AMPK in the border zones of the ischaemic hearts of control and adipocyte-specific *IP6K1* KO mice at 24 h after myocardial ischaemia-reperfusion injury. Data were presented as mean \pm SEM, Student's *t*-test, $n = 6$ mice per group. (H) Protein levels of cleaved caspase 3 in the border zones of the ischaemic hearts of control and adipocyte-specific *IP6K1* KO mice at 24 h after myocardial ischaemia-reperfusion injury. Data were presented as mean \pm SEM, Student's *t*-test, $n = 5$ mice per group.

3.4 IP6K1 bound to adiponectin

We tested whether IP6K1 regulates adiponectin transcription. The mRNA levels of adiponectin in adipocytes were similar between WT and *IP6K1* KO (see [Supplementary material online, Figure S4](#)), indicating that IP6K1 did not regulate adiponectin transcription.

To investigate the molecular mechanism by which IP6K1 regulated adiponectin, we performed immunoprecipitations of IP6K1 to look for its binding partners. Protein electrophoresis, silver staining, and mass spectrometry revealed that adiponectin was co-immunoprecipitated by IP6K1 in hearts, adipose tissues, and skeletal muscles of mice ([Figure 3A](#)), which was confirmed by western blots ([Figure 3B](#)). As a negative control, we show that immunoprecipitation of IP6K1 pulled down adiponectin in WT but not *IP6K1* KO preparations ([Figure 3C and D](#)). To rule out non-specific activity of the IP6K1 antibody, we overexpressed flag-tagged adiponectin and myc-tagged IP6K1 together and validated the IP6K1/adiponectin binding by immunoprecipitation of flag-tag and myc-tag ([Figure 3E and F](#)). IP6K2 and IP6K3 are two other isoforms of IP6Ks and share similar kinase activities with IP6K1. IP6K1 functions mainly in the cytosol and at the plasma membrane, while IP6K2 is primarily a nuclear protein. IP6K3 is highly expressed in heart and brain. We performed immunoprecipitations and western blots to test whether IP6K2 and IP6K3 interact with adiponectin. Immunoprecipitation of IP6K2 did not pull down adiponectin ([Figure 3G and H](#); see [Supplementary material online, Figure S5A](#)). IP6K3 and adiponectin did not bind each other ([Figure 3H](#); see [Supplementary material online, Figure S5B and C](#)). Thus, only IP6K1 bound to adiponectin.

We utilized the adipocyte-specific *IP6K1* KO mice (*adipoq*-cre; *IP6K1*^{fl/fl}) to examine the interaction of IP6K1 with adiponectin in the heart and adipose tissue ([Figure 3I and J](#)). Immunoprecipitations of IP6K1 in the heart co-pulled down similar amounts of adiponectin in the control (*IP6K1*^{fl/fl}) and adipocyte-specific *IP6K1* KO (*adipoq*-cre; *IP6K1*^{fl/fl}) animals, suggesting that the interaction of IP6K1 with adiponectin in the hearts was not affected by the deletion of IP6K1 in adipocytes ([Figure 3I](#)). In contrast, immunoprecipitations of IP6K1 in adipose tissues co-pulled down adiponectin in the control (*IP6K1*^{fl/fl}) mice but not in the adipocyte-specific *IP6K1* KO (*adipoq*-cre; *IP6K1*^{fl/fl}) mice ([Figure 3J](#)).

Adiponectin is secreted through the ER–Golgi pathway. To test whether IP6K1 is present in the ER–Golgi pathway, we performed immunostaining of IP6K1 and GRP78 for ER. Confocal microscopy revealed that IP6K1 was partially co-localized with GRP78 (see [Supplementary material online, Figure S6A](#)). We isolated the subcellular fraction of ER. Western blots showed that IP6K1 was present in the ER fraction (see [Supplementary material online, Figure S6B](#)).

3.5 5-InsP₇ enhanced the binding of adiponectin with ERp44

Thiol-mediated protein quality control by ERp44 is a key mechanism that governs adiponectin biosynthesis and permits tight regulation of circulating adiponectin levels.^{12–14} Deletion of IP6K1 reduced the binding of adiponectin with ERp44 ([Figure 4A and B](#)). Confocal microscopy also revealed that the co-localization of adiponectin with ERp44 was decreased in the *IP6K1* KO adipocytes ([Figure 4C](#)).

We performed immunoprecipitations to examine whether IP6K1 interacts with ERp44 (see [Supplementary material online, Figure S7](#)). The results showed that IP6K1 did not bind ERp44 (see [Supplementary material online, Figure S7](#)); thus, IP6K1 did not function as a scaffolding protein to mediate the interaction of adiponectin/ERp44.

To test whether 5-InsP₇ mediated the binding of adiponectin with ERp44, we utilized TNP, an IP6K inhibitor,³⁵ to block 5-InsP₇ biosynthesis in adipocytes. Immunoprecipitations and western blots revealed that adiponectin co-immunoprecipitated less ERp44 in TNP-treated cells ([Figure 4D](#)). Similarly, ERp44 co-immunoprecipitated less adiponectin when 5-InsP₇ biosynthesis was inhibited ([Figure 4E](#)), indicating that 5-InsP₇ was required for the interaction of adiponectin with ERp44. This result was further confirmed by utilizing SC-919 (see [Supplementary material online, Figure S8](#)), a selective IP6K inhibitor.²⁶

To test whether 5-InsP₇ bound adiponectin and/or ERp44, resin-bound 5PCP,³¹ a metabolically resistant analogue of 5-InsP₇, was used as a bait to

pull down adiponectin and ERp44 ([Figure 4F](#)). 5PCP was immobilized to the resin via a linker at the 1-, 2-, or 3-position in equal parts. A resin with monophosphate attached via the same linker was used as control.³¹ 5PCP-resin pulled down both endogenous adiponectin from adipocyte whole cell lysates ([Figure 4F](#)) and the purified adiponectin (see [Supplementary material online, Figure S9](#)). In contrast, 5PCP-resin did not pull down ERp44 ([Figure 4F](#)), suggesting that 5-InsP₇ bound adiponectin but not ERp44.

We performed an *in vitro* binding assay to test whether 5-InsP₇ could mediate the interaction of adiponectin with ERp44. Compared with InsP₆, the immediate precursor of 5-InsP₇, 5-InsP₇ enhanced the binding of adiponectin with ERp44 more strongly ([Figure 4G](#)). Two different non-hydrolysable analogues of 5-InsP₇, 5PCP³⁶ and CF2,²⁸ both strengthened the interaction of adiponectin with ERp44 ([Figure 4H](#)). We also used 'no InsP', Ins(14,5)P₃, Ins(1,3,4,5)P₄, and Ins(1,3,4,5,6)P₅ as controls to determine if the interaction was mediated simply by increased electrostatic charge. The *in vitro* binding results showed that 5-InsP₇ but not Ins(14,5)P₃, Ins(1,3,4,5)P₄, or Ins(1,3,4,5,6)P₅ enhanced the adiponectin/ERp44 interaction ([Figure 4I](#)). 1-InsP₇, 3-InsP₇, and 5-InsP₇ are inositol pyrophosphates with the pyrophosphate at 1-, 3-, and 5-positions of the inositol ring, respectively. The *in vitro* binding assay showed that 1-InsP₇ and 3-InsP₇ displayed weaker effects compared to 5-InsP₇ in mediating the adiponectin/ERp44 interaction ([Figure 4J](#)). The above results indicated that the interaction was due specifically to 5-InsP₇ but not simply increased electrostatic charge.

3.6 5-InsP₇ enhanced the binding of DsbA-L with Ero1- α

DsbA-L and Ero1- α form complexes with adiponectin and ERp44 and are critical regulators of thiol-mediated quality control of adiponectin biosynthesis.^{12,17,37} We performed immunoprecipitations and western blots to show that IP6K1 bound DsbA-L ([Figure 5A and B](#)) but not Ero1- α (see [Supplementary material online, Figure S10](#)). Although IP6K1 bound both adiponectin and DsbA-L, deletion of IP6K1 did not affect the interaction between adiponectin and DsbA-L (see [Supplementary material online, Figure S11](#)). In contrast, the interaction between DsbA-L and Ero1- α was reduced in *IP6K1* KO adipocytes ([Figure 5C and D](#)). Notably, IP6K1 did not function as a scaffolding protein to mediate the interaction of DsbA-L with Ero1- α because IP6K1 did not bind Ero1- α (see [Supplementary material online, Figure S10](#)).

We utilized 5PCP-resin to pull down DsbA-L and Ero1- α . The results showed that DsbA-L, but not Ero1- α , was pulled down by 5PCP-resin, indicating that 5-InsP₇ bound DsbA-L ([Figure 5E](#); see [Supplementary material online, Figure S12](#)), but not Ero1- α ([Figure 5E](#)). We performed an *in vitro* binding assay to examine whether 5-InsP₇ could mediate the interaction of DsbA-L with Ero1- α . InsP₆, the precursor of 5-InsP₇, was used as a control. Results showed that 5-InsP₇ enhanced the protein–protein interaction of DsbA-L with Ero1- α ([Figure 5F](#)). The two non-hydrolyzable analogues of 5-InsP₇, 5PCP and CF2, displayed similar effects to 5-InsP₇ in mediating the binding of DsbA-L with Ero1- α ([Figure 5G](#)).

We used 'no InsP', Ins(14,5)P₃, Ins(1,3,4,5)P₄, and Ins(1,3,4,5,6)P₅ as controls to test the specificity of 5-InsP₇ in mediating the interaction of DsbA-L with Ero1- α . Results showed that Ins(14,5)P₃ and Ins(1,3,4,5,6)P₅ did not enhance the binding in the *in vitro* binding assay ([Figure 5H](#)). However, Ins(1,3,4,5)P₄ displayed similar effects to 5-InsP₇ in mediating the interaction of DsbA-L with Ero1- α ([Figure 5H](#)). We also compared 5-InsP₇ with 1-InsP₇ and 3-InsP₇ in the *in vitro* binding assay ([Figure 5I](#)). Results demonstrated that 1-InsP₇ and 3-InsP₇ did not display similar effects to 5-InsP₇ in mediating the interaction of DsbA-L with Ero1- α ([Figure 5I](#)).

Neither IP6K1 nor its product 5-InsP₇ interacted with Ero1- α or ERp44 directly, and deletion of IP6K1 did not affect the binding of Ero1- α with ERp44 (see [Supplementary material online, Figure S13](#)).

3.7 5-InsP₇ elicited adiponectin intracellular degradation

Nearly 50% of newly synthesized adiponectin is degraded intracellularly via ERp44-dependent protein quality control,^{12,38} which might be regulated when the adiponectin–ERp44 interaction is disrupted by depleting 5-InsP₇. To address this possibility, we examined adiponectin protein levels

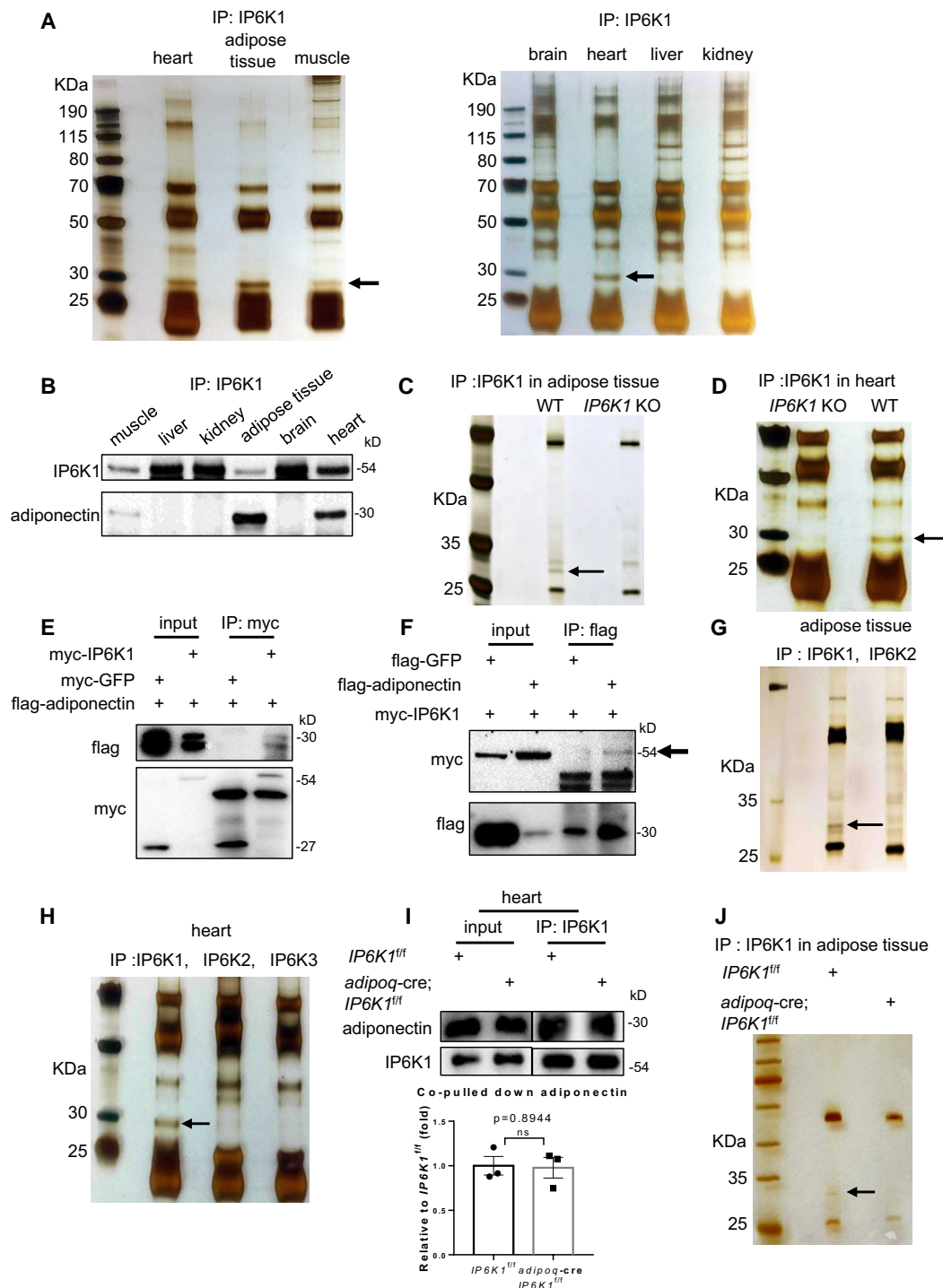


Figure 3 IP6K1 bound to adiponectin. (A) Immunoprecipitation of IP6K1 in mice tissues. Silver stain and mass spectrometry revealed that adiponectin (arrow) was co-pulled down by IP6K1 in the heart, adipose tissue, and skeletal muscle, but not in the brain, liver, or kidney. (B) Western blots showed that adiponectin was pulled down by IP6K1 in adipose tissue, heart, and skeletal muscle. (C) Immunoprecipitation of IP6K1 pulled down adiponectin (arrow) in WT but not *IP6K1* KO adipose tissues. (D) Pulling down IP6K1 co-immunoprecipitated adiponectin (arrow) in WT but not *IP6K1* KO hearts. (E) Myc-tagged IP6K1 and flag-tagged adiponectin were overexpressed together. Pulling down myc-tag IP6K1 co-immunoprecipitated flag-adiponectin. Myc-tagged GFP was used as a negative control. (F) Flag-tagged adiponectin and myc-tagged IP6K1 were overexpressed together. Pulling down flag-tagged adiponectin co-immunoprecipitated myc-IP6K1 (arrow). Flag-tagged GFP was used as a negative control. (G) Adiponectin (arrow) was co-pulled down by IP6K1 but not IP6K2 in WT adipose tissues. (H) Adiponectin (arrow) was co-immunoprecipitated by IP6K1 but not IP6K2 or IP6K3 in WT hearts. (I) Immunoprecipitations of IP6K1 co-pulled down similar amounts of adiponectin in the hearts of control (*IP6K1*^{fl/fl}) and adipocyte-specific *IP6K1* KO (*adipoq*-cre; *IP6K1*^{fl/fl}) mice. Data were presented as mean \pm SEM, Student's *t*-test, *n* = 3. (J) Immunoprecipitation of IP6K1 co-pulled down adiponectin (arrow) in adipose tissues of control (*IP6K1*^{fl/fl}) but not adipocyte-specific *IP6K1* KO mice (*adipoq*-cre; *IP6K1*^{fl/fl}).

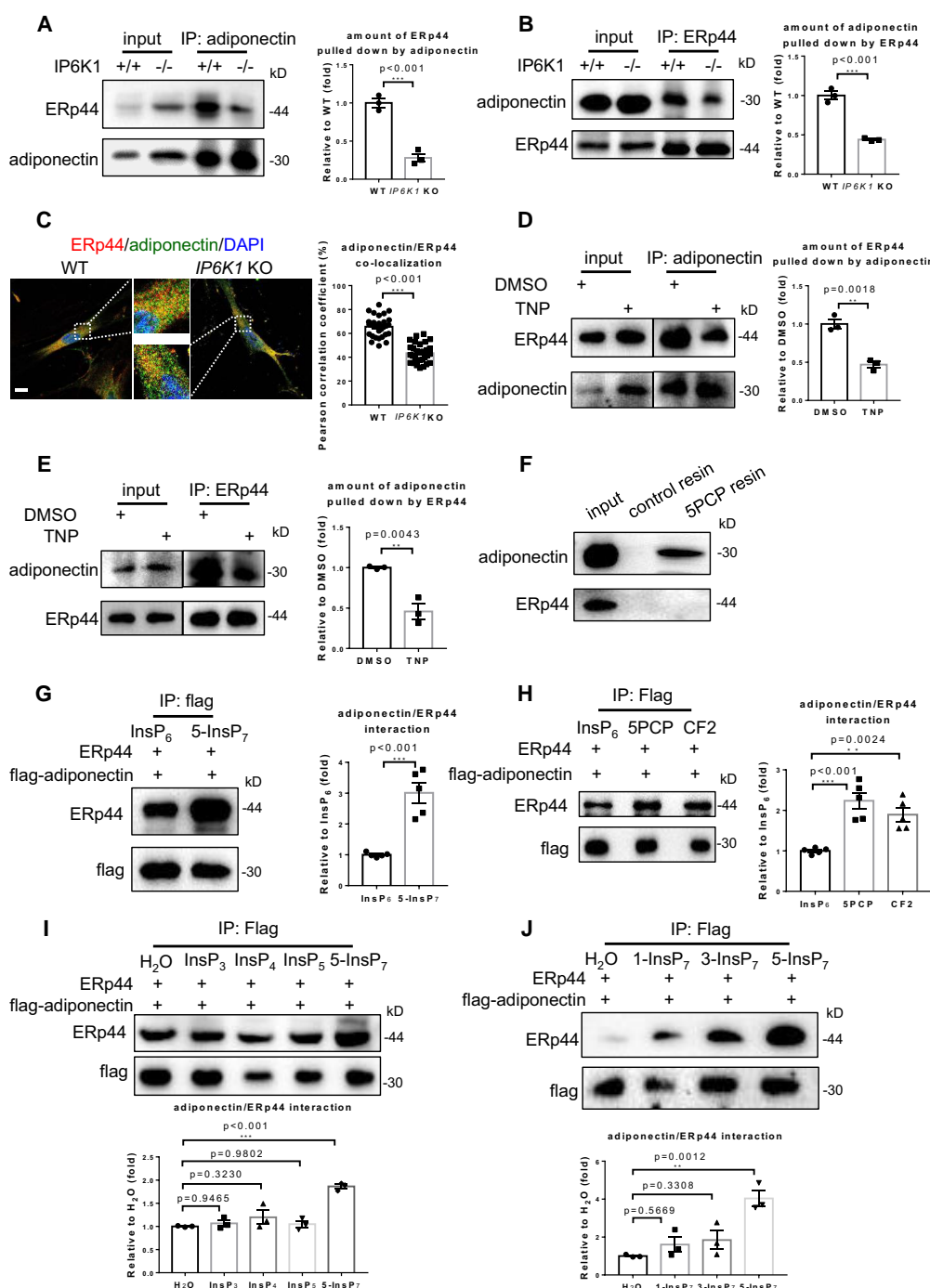


Figure 4 5-InsP₇ enhanced the binding of adiponectin with ERp44. (A) Immunoprecipitation of adiponectin pulled down less ERp44 in *IP6K1* KO adipose tissues. Data were presented as mean \pm SEM, Student's *t*-test, $n = 3$ independent repeats. (B) Pulling down ERp44 co-immunoprecipitated less adiponectin in *IP6K1* KO adipose tissues. Data were presented as mean \pm SEM, Student's *t*-test, $n = 3$ independent repeats. (C) Immunostaining of adiponectin and ERp44 in WT and *IP6K1* KO adipocytes. The co-localization of ERp44 and adiponectin was decreased in *IP6K1* KO adipocytes. Data were presented as means \pm SEM from 30 images of three independent experiments. Student's *t*-test. Scale bar: 10 μ m. (D, E) 3T3-L1 adipocytes were treated with TNP (3 μ M for 24 h) to block 5-InsP₇ synthesis. Immunoprecipitation of adiponectin or ERp44 pulled down less of each other in the TNP-treated cells than in the DMSO-treated control cells. Data were presented as mean \pm SEM, Student's *t*-test, $n = 3$ independent repeats. (F) 5PCP-resin pulled down endogenous adiponectin but not ERp44 in whole cell lysates of adipocytes. (G) Compared with InsP₆, 5-InsP₇ enhanced the interaction of adiponectin with ERp44 in an *in vitro* binding assay. Data were presented as mean \pm SEM, Student's *t*-test, $n = 5$ independent repeats. (H) Both 5PCP and CF2 promoted the binding of adiponectin with ERp44 in an *in vitro* binding assay. Data were presented as mean \pm SEM, one-way ANOVA, $n = 5$ independent repeats. (I) 5-InsP₇ but not InsP₃, InsP₄, or InsP₅ enhanced the binding of adiponectin with ERp44. Data were presented as mean \pm SEM, one-way ANOVA, $n = 3$ independent repeats. (J) 1-InsP₇ and 3-InsP₇ did not display similar effects to 5-InsP₇ in mediating the binding of adiponectin with ERp44. Data were presented as mean \pm SEM, one-way ANOVA, $n = 3$ independent repeats.

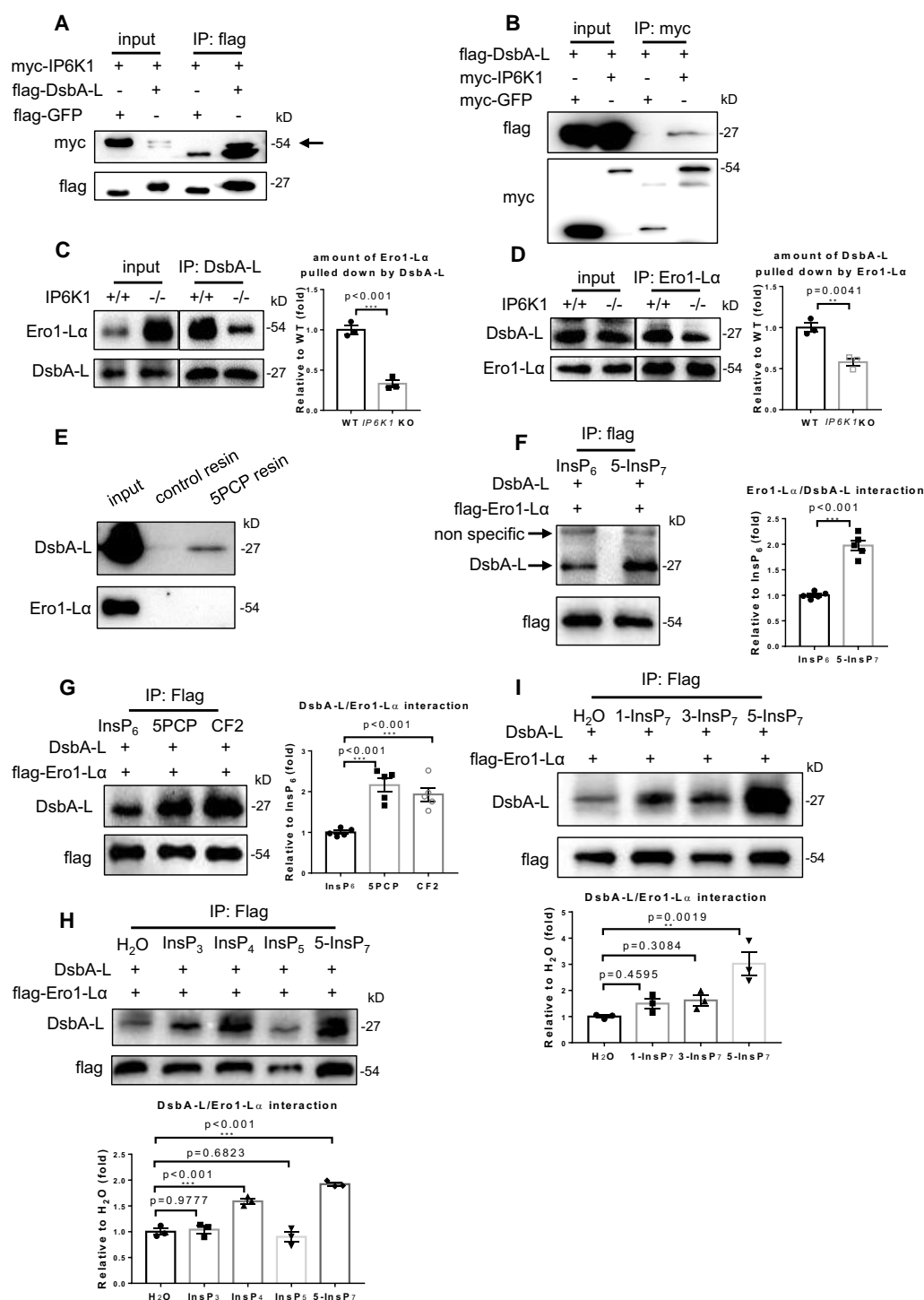


Figure 5 5-InsP₇ enhanced the binding of DsbA-L with Ero1-Lα. (A, B) Myc-IP6K1 and flag-DsbA-L were overexpressed together. (A) Immunoprecipitation of flag-tag DsbA-L co-pulled down myc-IP6K1 (arrow). Flag-GFP was used as a negative control. (B) Immunoprecipitation of myc-tag IP6K1 co-pulled down flag-DsbA-L. Myc-GFP was used as a negative control. (C) Immunoprecipitation of DsbA-L pulled down less Ero1-Lα in IP6K1 KO adipocytes than in WT. Data were presented as mean ± SEM, Student's *t*-test, *n* = 3 independent repeats. (D) Pulling down Ero1-Lα co-immunoprecipitated less DsbA-L in IP6K1 KO adipocytes than in WT. Data were presented as mean ± SEM, Student's *t*-test, *n* = 3 independent repeats. (E) 5PCP-resin pulled down endogenous DsbA-L but not Ero1-Lα in the whole cell lysates of adipocytes. (F) Compared with InsP₆, 5-InsP₇ enhanced the interaction of Ero1-Lα with DsbA-L in an *in vitro* binding assay. Data were presented as mean ± SEM, Student's *t*-test, *n* = 5 independent repeats. (G) Both 5PCP and CF2 promoted the binding of Ero1-Lα with DsbA-L in an *in vitro* binding assay. Data were presented as mean ± SEM, one-way ANOVA, *n* = 5 independent repeats. (H) 5-InsP₇ and InsP₄ but not InsP₃ or InsP₅ enhanced the binding of Ero1-Lα with DsbA-L. Data were presented as mean ± SEM, one-way ANOVA, *n* = 3 independent repeats. (I) 1-InsP₇ and 3-InsP₇ did not display similar effects to 5-InsP₇ in mediating the binding of Ero1-Lα with DsbA-L. Data were presented as mean ± SEM, one-way ANOVA, *n* = 3 independent repeats.

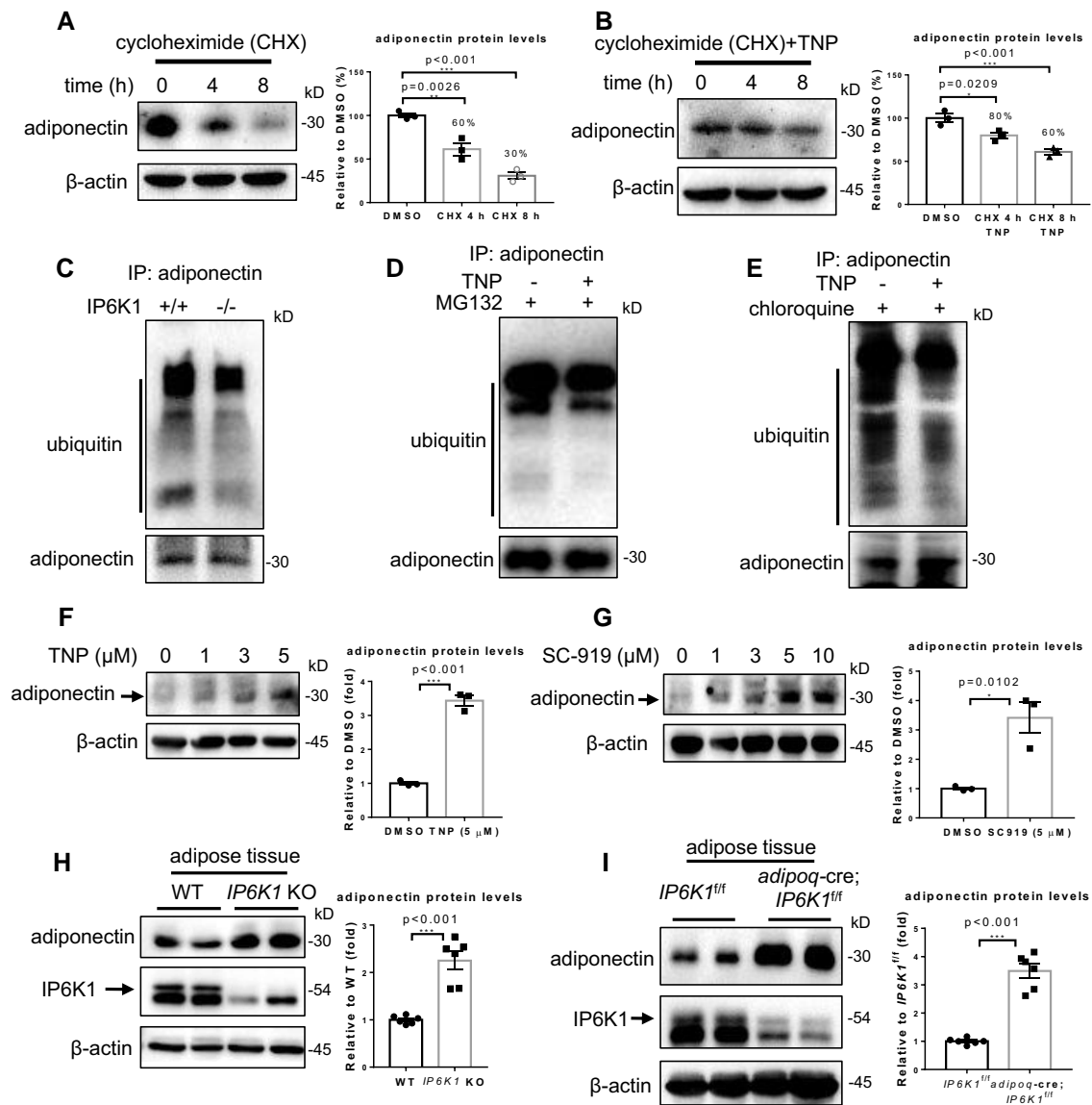


Figure 6 5-InsP₇ elicited adiponectin intracellular degradation. (A, B) 3T3-L1 adipocytes were treated with cycloheximide (CHX, 100 μM) to block protein synthesis. (A) Adiponectin protein levels were determined by western blots. Data were presented as mean ± SEM, one-way ANOVA, $n = 3$ independent repeats. (B) Cells were co-treated with TNP (3 μM) to block 5-InsP₇ synthesis. Adiponectin protein levels were determined by western blots. Data were presented as mean ± SEM, one-way ANOVA, $n = 3$ independent repeats. (C) Adiponectin was immunoprecipitated in WT and *IP6K1* KO adipose tissues and blotted for ubiquitin. (D) 3T3-L1 adipocytes were treated with TNP (3 μM for 24 h) to block 5-InsP₇ synthesis followed by MG132 treatment (10 μM for 4 h) to block proteasomal degradation. Adiponectin was immunoprecipitated and blotted for ubiquitin. (E) 3T3-L1 adipocytes were treated with TNP (3 μM for 24 h) to block 5-InsP₇ synthesis followed by chloroquine treatment (50 μM for 24 h) to block autophagy. Adiponectin was immunoprecipitated and blotted for ubiquitin. (F) 3T3-L1 adipocytes were treated with TNP for 24 h. Adiponectin (arrow) protein levels were determined by western blots. Data were presented as mean ± SEM, Student's *t*-test, $n = 3$ independent repeats. (G) 3T3-L1 adipocytes were treated with SC-919 for 24 h. Adiponectin (arrow) protein levels were determined by western blots. Data were presented as mean ± SEM, Student's *t*-test, $n = 3$ independent repeats. (H) Adiponectin protein levels in WT and *IP6K1* KO adipose tissues. Arrow points to *IP6K1*. Data were presented as mean ± SEM, Student's *t*-test, $n = 6$ mice per group. (I) Adiponectin protein levels in the adipose tissues of control (*IP6K1*^{fl/fl}) and adipocyte-specific *IP6K1* KO mice (*adipoq*-cre; *IP6K1*^{fl/fl}). Arrow points to *IP6K1*. Data were presented as mean ± SEM, Student's *t*-test, $n = 6$ mice per group.

in 3T3-L1 adipocytes when *de novo* protein synthesis was inhibited by cycloheximide. Results showed that adiponectin protein levels were rapidly reduced when *de novo* protein synthesis was inhibited by cycloheximide (Figure 6A), but the half-life of adiponectin was longer when 5-InsP₇ was depleted by TNP treatment (Figure 6B).

We compared the adiponectin degradation *in vivo* by examining its ubiquitination levels in WT and *IP6K1* KO adipose tissues. Equal amounts of adiponectin were immunoprecipitated from WT and *IP6K1* KO adipose

tissues and blotted for ubiquitin. Results showed that the adiponectin ubiquitination levels were lower in *IP6K1* KO preparations than those of WT, indicating less degradation of adiponectin in the *IP6K1* KO adipocytes (Figure 6C). Proteasomal and lysosomal activities are known to mediate adiponectin intracellular degradation.³⁹ We utilized MG132 and chloroquine to block proteasomal and lysosomal activities, respectively, and tested whether inhibiting 5-InsP₇ synthesis could affect adiponectin ubiquitin levels (Figure 6D and E). Immunoprecipitation and western blots showed

that inhibiting 5-InsP₇ synthesis by TNP treatment decreased adiponectin ubiquitination levels (Figure 6D and E). This was confirmed by using another IP6K inhibitor, SC-919 (see [Supplementary material online, Figure S14](#)). In contrast, the adiponectin protein levels in adipocytes were elevated when 5-InsP₇ synthesis is inhibited by either TNP or SC-919 (Figure 6F and G). The adiponectin protein levels were higher in the adipose tissues of IP6K1 KO mice than those of WT littermates (Figure 6H). Similarly, adiponectin protein levels were higher in the adipose tissues of adipocyte-specific IP6K1 KOs (*adipoq-cre; IP6K1^{fl/fl}*) than those of controls (*IP6K1^{fl/fl}*; Figure 6I).

Metabolic dysfunction is linked to decreased levels of adiponectin in the bloodstream. To determine if IP6K1 expression levels are altered in this pathological condition, we compared its expression levels in adipose tissues of obese (*ob/ob*) and non-obese control mice. Western blots showed that the protein levels of IP6K1 were higher in the adipose tissues of obese (*ob/ob*) mice (see [Supplementary material online, Figure S15A](#)), which may contribute to the decreased levels of adiponectin. The expression levels of adiponectin follow a circadian rhythm.^{40,41} We collected the adipose tissues at different time points of a 24 h period to test whether the expression of IP6K1 might show daily circadian rhythms. The IP6K1 protein levels were similar, indicating that it did not regulate adiponectin's circadian rhythm (see [Supplementary material online, Figure S15B](#)).

3.8 Pharmacological inhibition of 5-InsP₇ biosynthesis attenuated myocardial ischaemia–reperfusion injury in WT but not adiponectin KO animals

To evaluate the role of 5-InsP₇ in regulating adiponectin *in vivo*, TNP was administered to WT mice to block 5-InsP₇ biosynthesis. Although no obvious accumulation of adiponectin in adipose tissues was observed (see [Supplementary material online, Figure S16](#)), the plasma levels of HMW adiponectin were elevated after TNP treatment (Figure 7A). To test whether pharmacological inhibition of 5-InsP₇ biosynthesis could ameliorate myocardial ischaemia–reperfusion injury, animals were treated with TNP for 1 week and then subjected to cardiac ischaemia–reperfusion injury. Results showed that the infarct size was smaller in the TNP-treated mice than that of vehicle-treated controls (Figure 7B).

We utilized *adiponectin* KO mice to validate whether adiponectin mediates the protective effect of IP6K1 inhibition. We were unable to generate the *IP6K1/adiponectin* double KO mice by crossing the *IP6K1* KO mice with *adiponectin* KO mice. Knocking out IP6K1 together with adiponectin may cause reproduction defects because deletion of IP6K1 elicits male infertility,^{42,43} and deletion of adiponectin affects both male and female reproductive systems.⁴⁴ As an alternative, we utilized TNP administration to block 5-InsP₇ synthesis in *adiponectin* KO mice. Adiponectin protein was absent in both adipose tissues and plasma of *adiponectin* KO mice (Figure 7C and D). Deletion of adiponectin compromised the protective effects of TNP against myocardial ischaemia–reperfusion injury (Figure 7E), indicating that the cardioprotective effects of IP6K1 inhibition required endogenous adiponectin.

4. Discussion

Increased levels of IP6K1 protein and its product 5-InsP₇ are implicated in aging and disease, and inhibiting IP6K1-mediated 5-InsP₇ biosynthesis provides therapeutic benefits.^{21,22,45} We explored the role of IP6K1/5-InsP₇ in cardiac ischaemia–reperfusion injury and found that deletion of IP6K1 or pharmacological inhibition of 5-InsP₇ biosynthesis could attenuate myocardial infarction by elevating plasma adiponectin levels. IP6K1 bound adiponectin and DsbA-L, a critical chaperone for adiponectin biosynthesis. Deletion of IP6K1 disrupted the interactions of the adiponectin/DsbA-L complex with the ERp44/Ero1- α complex (Figure 8). IP6K1 generates a local pool of 5-InsP₇, which strengthened adiponectin/DsbA-L binding to ERp44/Ero1- α , and caused intracellular retention and degradation of

adiponectin. Depleting 5-InsP₇ by either knocking out IP6K1 or pharmacological inhibition of IP6K1 kinase activity allowed adiponectin to avoid ERp44-mediated degradation (Figure 8). In addition, whole-body and adipocyte-specific deletion of IP6K1 elevated circulating adiponectin protein levels, particularly the HMW forms, and protected the heart from myocardial ischaemia–reperfusion injury. Pharmacological inhibition of 5-InsP₇ biosynthesis attenuated myocardial ischaemia–reperfusion injury in WT but not *adiponectin* KO mice confirming that adiponectin mediated the cardioprotective effects of IP6K1 inhibition. Our study demonstrates that IP6K1 could be a potential therapeutic target for ischaemic heart disease and reveals a mechanism whereby IP6K1/5-InsP₇ governs circulating adiponectin levels.

Adiponectin exerts pleiotropic protective effects. Low plasma levels of adiponectin are in part responsible for the pathogenesis of cardiovascular diseases in obese and diabetic patients. Replenishing adiponectin appears to be a promising therapeutic strategy. However, due to its high basal concentration and rapid elimination, exogenous adiponectin administration remains challenging.^{8–10} Ubiquitin pathway-mediated adiponectin intracellular degradation is a major contributor of reduced circulating adiponectin.^{46–48} Preventing futile intracellular degradation of adiponectin is an alternative strategy to boost adiponectin blood levels. ERp44, Ero1- α , and DsbA-L are chaperones that modulate adiponectin multimerization, retention, and secretion.^{12–17} Interactions of these molecules are required for adiponectin biosynthesis. However, on the other hand, the binding of ERp44 to adiponectin is also responsible for the intracellular degradation of adiponectin, although the mechanisms have not been fully delineated. Results from our study indicated that IP6K1 via its product 5-InsP₇ strengthened the interactions of ERp44/adiponectin/Ero1- α /DsbA-L, which led to adiponectin degradation. Releasing adiponectin from the interaction with ERp44 represents one of the rate-limiting steps for its secretion and effectively elevates plasma adiponectin levels.^{49–51} Consistently, our study demonstrated that depleting 5-InsP₇ was able to release adiponectin from binding with ERp44 and thereby elevated plasma adiponectin levels. Therefore, IP6K1-generated 5-InsP₇ might represent a molecular target to boost plasma adiponectin levels.

In this study, we demonstrated that administering the IP6K inhibitor TNP could protect the heart from myocardial ischaemia–reperfusion injury in mice. Our TNP administration paradigm aimed to show that 5-InsP₇ specifically, not IP6K1's non-enzymatic functions, raised adiponectin and that the resulting increase in circulating adiponectin protected the heart from myocardial ischaemia–reperfusion injury *in vivo*. For clinical application, it is ideal to administer pharmacological agents after myocardial ischaemia injury. Future studies are needed to determine if administering IP6K inhibitors after myocardial ischaemia is still effective and to understand its mechanisms.

Recently, it has been proposed that the increased insulin sensitivity in *IP6K1* KO mice may come from enhanced adiponectin signalling.^{23,52} While this suggests a possibility that IP6K1 or 5-InsP₇ might be involved in modulating adiponectin biosynthesis, the mechanism and physiological relevance were not elucidated in these studies. Our study revealed that IP6K1 generates a local pool of 5-InsP₇ to elicit adiponectin intracellular retention and degradation via mediating the formation of an adiponectin/ERp44/DsbA-L/Ero1- α complex (Figure 8). Knocking out IP6K1 or pharmacological inhibition of IP6K1 kinase activity could prevent adiponectin intracellular degradation and boost its biosynthesis, which activated the AMPK signalling pathway in the heart and protected cardiomyocytes from ischaemic death. The 5-InsP₇-enhanced adiponectin/ERp44 and DsbA-L/Ero1- α interactions were unlikely to involve protein pyrophosphorylation by 5-InsP₇, because the effects were recapitulated by synthetic non-hydrolyzable analogues of 5-InsP₇ that cannot transfer a phosphate group. The enhanced protein–protein interactions were due specifically to 5-InsP₇ but not simply by increased electrostatic charge, because 1-InsP₇ and 3-InsP₇ were much less effective. Ins(14,5)P₃ and Ins(1,3,4,5,6)P₅ did not display similar effects to 5-InsP₇; however, Ins(1,3,4,5)P₄ was able to enhance the binding of DsbA-L with Ero1- α , whose mechanism was not clear. There might be a common structural mechanism that is shared between Ins(1,3,4,5)P₄ and 5-InsP₇. The detailed structural mechanisms of

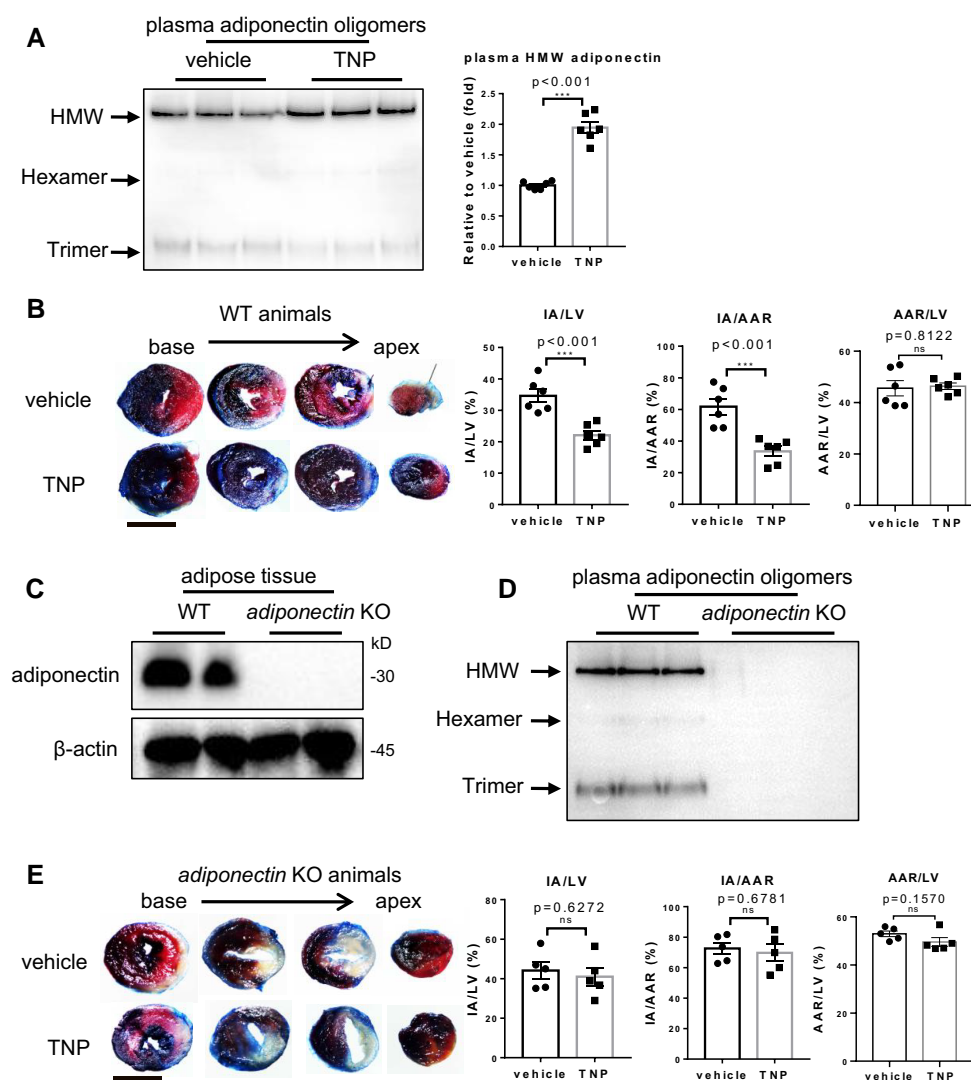


Figure 7 Pharmacological inhibition of 5-InsP₇ biosynthesis attenuated ischaemia–reperfusion injury in WT but not *adiponectin* KO mice. (A) WT animals were injected with TNP for 1 week. The plasma adiponectin oligomers (arrows) were determined by western blots. Data were presented as mean ± SEM, Student's *t*-test, *n* = 6 mice per group. (B) Evans blue and TTC double staining of the hearts after ischaemia–reperfusion injury. The non-ischaemic area is indicated by blue, the area at risk (AAR) by red and white, and the infarct area (IA) by white. LV, left ventricle. Data were presented as mean ± SEM, Student's *t*-test, *n* = 6 mice per group. Scale bar: 5 mm. (C) Adiponectin protein levels in adipose tissues of WT and *adiponectin* KO mice, *n* = 4 mice per group. (D) Plasma adiponectin oligomers (arrows) in WT and *adiponectin* KO mice, *n* = 3 mice per group. (E) *Adiponectin* KO mice were injected with TNP for 1 week and were subjected to ischaemia–reperfusion injury. The ischaemia–reperfusion injured hearts were stained with Evans blue and TTC. The non-ischaemic area is indicated by blue, the AAR by red and white, the IA by white. LV, left ventricle. Data were presented as mean ± SEM, ns = not significant, Student's *t*-test, *n* = 5 mice per group. Scale bar: 5 mm.

5-InsP₇-mediated adiponectin/ERp44 and DsbA-L/Ero1- α interactions warrant future studies. Depleting 5-InsP₇ reduces the level of 1,5-bis-diphosphoinositol 2,3,4,6-tetrakisphosphate (1,5-InsP₈), which possesses two pyrophosphates at both 1- and 5-positions of the inositol ring.⁵³ We did not exclude the possibility that 1,5-InsP₈ could also bind adiponectin or DsbA-L. However, the physiological concentration of 5-InsP₇ is far higher than that of 1,5-InsP₈⁵⁴; besides, the weak activity of 1-InsP₇ makes it unlikely that 1,5-InsP₈ will bind better than 5-InsP₇.⁵⁵ InsP₆ has been shown to have anti-oxidant properties, which might be enriched in *IP6K1* KO mice.⁵⁶ However, 5-InsP₇ displays better effects than InsP₆ in mediating the binding of adiponectin with ERp44 and the binding of DsbA-L with Ero1- α . Therefore, 5-InsP₇, not InsP₆, is likely a physiological regulator of adiponectin.

Circulating adiponectin is predominantly produced by adipocytes, but it also is expressed in cardiomyocytes and skeletal muscle cells.^{7,57} The regulatory mechanisms of cardiomyocyte-derived adiponectin have been elusive and may be different to those in adipocytes.^{58,59} Our study revealed that deletion of *IP6K1* elevated adiponectin protein levels in adipocytes but not in cardiomyocytes, although *IP6K1* bound adiponectin in both adipocytes and cardiomyocytes. The physiological functions of *IP6K1*/adiponectin interaction in cardiomyocytes are currently unknown. *IP6K1* has been proposed as a potential therapeutic target for treating diseases, including cardiovascular disease.²² *IP6K1* protein levels and activity are modulated by energy status. For instance, an increased ATP/ADP ratio enhances *IP6K1* activity. However, its functions and mechanisms in cardiomyocytes remain to be delineated.²² It has been reported that inhibiting

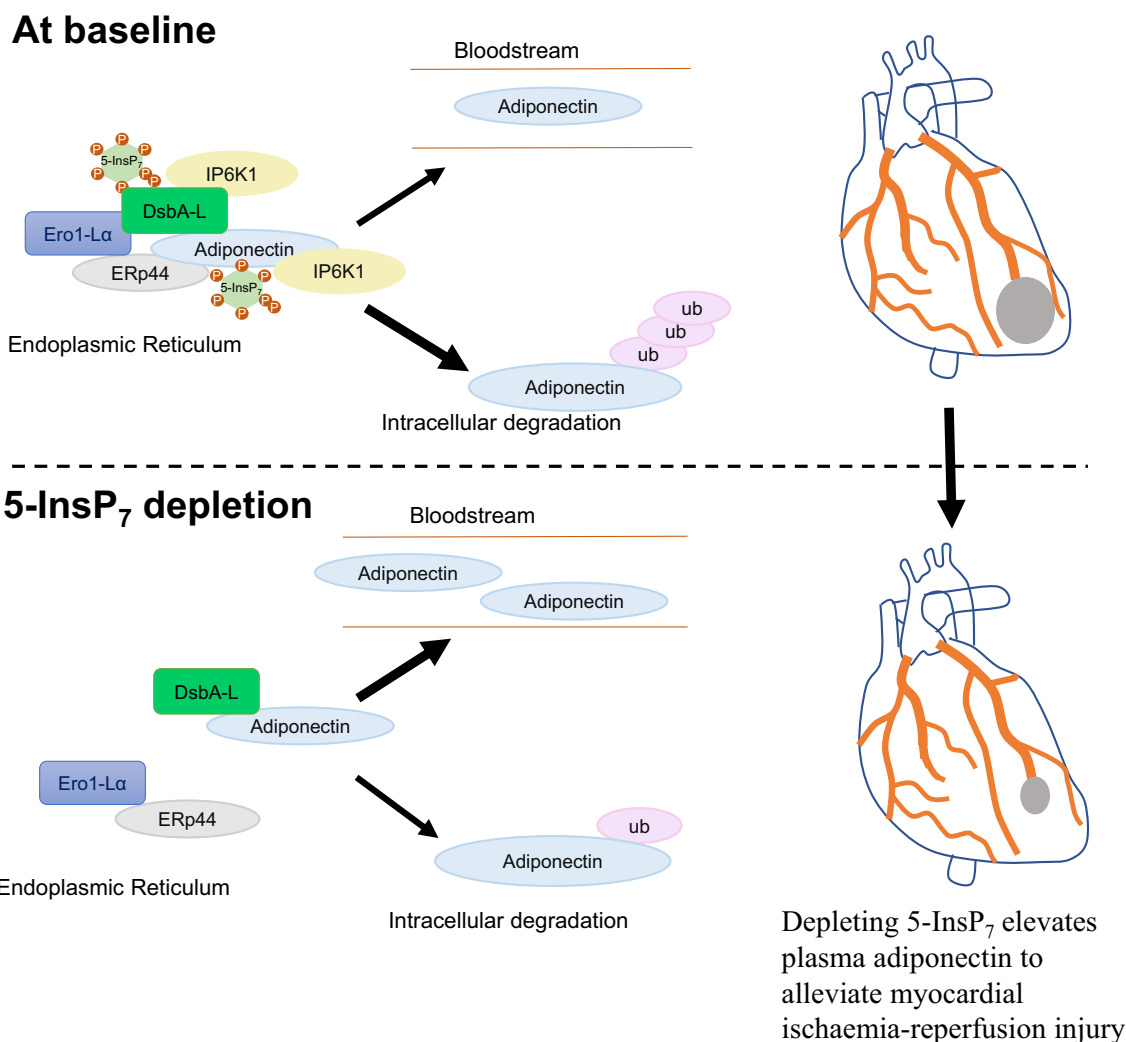


Figure 8 Model for 5-InsP₇ regulation of the intracellular fate of adiponectin. Upper panel: IP6K1 physiologically associates with the adiponectin/DsbA-L complex and generates a local pool of 5-InsP₇, which binds adiponectin and DsbA-L to enhance the interaction of the adiponectin/DsbA-L complex with the ERp44/Ero1-Lα complex. As a result, adiponectin is retained and degraded intracellularly. Lower panel: Depleting 5-InsP₇ disrupts the binding between the adiponectin/DsbA-L complex with the ERp44/Ero1-Lα complex, which releases adiponectin into the secretory pathway. Depleting 5-InsP₇ could protect the heart from myocardial ischaemia-reperfusion injury by boosting plasma adiponectin.

5-InsP₇ biosynthesis by TNP treatment protects cardiomyocytes from ischaemia-reperfusion injury, but the mechanism remains elusive.²⁴ Our study also demonstrated that TNP treatment attenuated myocardial ischaemia-reperfusion injury. The TNP-mediated protective effects required endogenous adiponectin, because TNP treatment alleviated ischaemia-reperfusion injury in WT but not *adiponectin* KO mice, indicating that the cardioprotective effect of TNP was attributable to the elevated adiponectin levels elicited by inhibiting 5-InsP₇ biosynthesis.

Adiponectin is a natural molecule that protects hearts from ischaemia-reperfusion injury. Ischaemia-reperfusion in adiponectin-deficient mice resulted in increased myocardial infarct size.^{4,60} In contrast, increasing adiponectin levels are associated with beneficial effects in both young and old mice.⁶¹ In low-risk patients, higher levels of adiponectin exert cardioprotective effects.^{62,63} Paradoxically, higher levels of adiponectin are associated with a higher mortality rate in patients with cardiovascular and metabolic disorders. The high levels of adiponectin may result from adiponectin resistance, thus reflecting a compensatory response in an attempt to restore heart function, rather than accelerating the disease progression.^{3,62}

Whether inhibition of IP6K1 provides long-term cardiovascular benefits remains to be investigated.

Adiponectin plasma levels are substantially higher in females than in males.⁶⁴ As females are less sensitive to myocardial ischaemia injury, we used male animals in this study to explore the impact of inhibiting IP6K1 on elevating plasma adiponectin and reducing myocardial ischaemia injury. The impact of inhibiting IP6K1 on myocardial ischaemia injury in females necessitates a comprehensive study.

In this study, we found that IP6K1 was present in the ER. IP6K1 has been found to affect the Golgi apparatus via its product 5-InsP₇.^{65,66} Multiple inositol polyphosphate phosphatase 1 is an ER resident and hydrolyses InsP₅, InsP₆, and 5-InsP₇ in the ER-Golgi apparatus biosynthetic-secretory pathway.⁶⁷⁻⁷¹ Taken together, these findings suggest that 5-InsP₇ and other higher InsPs play important roles in the ER and Golgi apparatus. Their functions and molecular mechanisms warrant further studies.

Our results are in agreement with a previous report that the plasma adiponectin concentration inversely correlates with body fat mass,⁷² because IP6K1 KO mice have reduced fat tissue content (see [Supplementary](#)

material online, Figure S17). This is in striking contrast to leptin, the plasma concentrations of which have been found to be lower in IP6K1 KO animals.^{21,73} A genetic study has linked IP6K1 with human obesity,⁷⁴ and IP6K1 expression levels are elevated in obese individuals,⁷⁵ which may contribute to the reduction of adiponectin under conditions of obesity. In contrast, global and adipocyte-specific knocking out of IP6K1 increase insulin sensitivity and energy expenditure and protect experimental animals from high-fat-diet-induced obesity.^{21,23,73}

Depletion of 5-InsP₇ by inhibiting IP6K1 simultaneously elevated adiponectin and reduced leptin levels, which could be an ideal strategy to treat cardiovascular disorders.³ IP6K1 has been proposed to be a potential therapeutic target for diabetes and chronic kidney diseases.^{23,26,73} Our findings suggest that IP6K1 might be a candidate drug target for treating ischaemic heart diseases.

Supplementary material

Supplementary material is available at *Cardiovascular Research* online.

Author contributions

Conceptualization: L.F., Y.Z. and C.F. Investigation: L.F., J.D., and X.L. Material support: Da.F., M.L.S., T.A., A.M.R., B.V.L.P., and Do.F. Funding acquisition: Y.Z. and C.F. Data analysis: L.F., J.D., X.Z., and C.F. Writing: A.C.C. and C.F. All authors reviewed and commented on this manuscript.

Conflict of interest: None declared.

Funding

This research was supported by the National Natural Science Foundation of China (82070259, 82330012, and 82220108021) and Natural Science Foundation of Shanghai (22ZR1440700). A.C.C. was supported by NIH Medical Scientist Training Program Training Grant T32GM007739 and an American Heart Association Predoctoral Fellowship. B.V.L.P. is a Wellcome Trust Senior Investigator (grant 101010). This research was funded in part by the Wellcome Trust. For the purpose of open access, the authors have applied a CC BY public copyright licence to any Author Accepted Manuscript version arising from this submission.

Data availability

All data are available in the main text or the supplementary materials.

References

1. Straub LG, Scherer PE. Metabolic messengers: adiponectin. *Nat Metab* 2019;**1**:334–339.
2. Stern JH, Rutkowski JM, Scherer PE. Adiponectin, leptin, and fatty acids in the maintenance of metabolic homeostasis through adipose tissue crosstalk. *Cell Metab* 2016;**23**:770–784.
3. Zhao S, Kusminski CM, Scherer PE. Adiponectin, leptin and cardiovascular disorders. *Circ Res* 2021;**128**:136–149.
4. Shibata R, Sato K, Pimentel DR, Takemura Y, Kihara S, Ohashi K, Funahashi T, Ouchi N, Walsh K. Adiponectin protects against myocardial ischemia-reperfusion injury through AMPK- and COX-2-dependent mechanisms. *Nat Med* 2005;**11**:1096–1103.
5. Fang H, Judd RL. Adiponectin regulation and function. *Compr Physiol* 2018;**8**:1031–1063.
6. Holland VL, Miller RA, Wang ZV, Sun K, Barth BM, Bui HH, Davis KE, Bikman BT, Halberg N, Rutkowski JM, Wade MR, Tenorio VM, Kuo MS, Brozinick JT, Zhang BB, Birnbaum MJ, Summers SA, Scherer PE. Receptor-mediated activation of ceramidase activity initiates the pleiotropic actions of adiponectin. *Nat Med* 2011;**17**:55–63.
7. Maeda N, Funahashi T, Matsuzawa Y, Shimomura I. Adiponectin, a unique adipocyte-derived factor beyond hormones. *Atherosclerosis* 2020;**292**:1–9.
8. Halberg N, Schraw TD, Wang ZV, Kim JY, Yi J, Hamilton MP, Luby-Phelps K, Scherer PE. Systemic fate of the adipocyte-derived factor adiponectin. *Diabetes* 2009;**58**:1961–1970.
9. Parida S, Siddharth S, Sharma D. Adiponectin, obesity, and cancer: clash of the bigwigs in health and disease. *Int J Mol Sci* 2019;**20**:2519.
10. Ruan H, Dong LQ. Adiponectin signaling and function in insulin target tissues. *J Mol Cell Biol* 2016;**8**:101–109.
11. Wang ZV, Scherer PE. Adiponectin, the past two decades. *J Mol Cell Biol* 2016;**8**:93–100.
12. Wang ZV, Schraw TD, Kim JY, Khan T, Rajala MW, Follenzi A, Scherer PE. Secretion of the adipocyte-specific secretory protein adiponectin critically depends on thiol-mediated protein retention. *Mol Cell Biol* 2007;**27**:3716–3731.
13. Anelli T, Sitia R. Protein quality control in the early secretory pathway. *EMBO J* 2008;**27**:315–327.
14. Tempio T, Anelli T. The pivotal role of ERp44 in patrolling protein secretion. *J Cell Sci* 2020;**133**:jcs240366.
15. Watanabe S, Amagai Y, Sannino S, Tempio T, Anelli T, Harayama M, Masui S, Sorrentino I, Yamada M, Sitia R, Inaba K. Zinc regulates ERp44-dependent protein quality control in the early secretory pathway. *Nat Commun* 2019;**10**:603.
16. Qiang L, Wang H, Farmer SR. Adiponectin secretion is regulated by SIRT1 and the endoplasmic reticulum oxidoreductase Ero1-L alpha. *Mol Cell Biol* 2007;**27**:4698–4707.
17. Liu M, Zhou L, Xu A, Lam KSL, Wetzel MD, Xiang R, Zhang J, Xin X, Dong LQ, Liu F. A disulfide-bond A oxidoreductase-like protein (DsbA-L) regulates adiponectin multimerization. *Proc Natl Acad Sci USA* 2008;**105**:18302–18307.
18. Chakraborty A. The inositol pyrophosphate pathway in health and diseases. *Biol Rev* 2018;**93**:1203–1227.
19. Shears SB, Wang H. Metabolism and functions of inositol pyrophosphates: insights gained from the application of synthetic analogues. *Molecules* 2020;**25**:4515.
20. Chin AC, Gao Z, Riley AM, Furkert D, Wittwer C, Dutta A, Rojas T, Semenza ER, Felder RA, Pluznick JL, Jessen HJ, Fiedler D, Potter BVL, Snyder SH, Fu C. The inositol pyrophosphate 5-InsP₇ drives sodium-potassium pump degradation by relieving an autoinhibitory domain of PI3K p85alpha. *Sci Adv* 2020;**6**:eabb8542.
21. Mukherjee S, Haubner J, Chakraborty A. Targeting the inositol pyrophosphate biosynthetic enzymes in metabolic diseases. *Molecules* 2020;**25**:1403.
22. Qi J, Shi L, Zhu L, Chen Y, Zhu H, Cheng W, Chen AF, Functions FC. Mechanisms, and therapeutic applications of the inositol pyrophosphates 5PP-InsP₅ and InsP₆ in mammalian cells. *J Cardiovasc Transl Res* 2023. Online ahead of print.
23. Zhu Q, Ghoshal S, Rodrigues A, Gao S, Asterian A, Kamenecka TM, Barrow JC, Chakraborty A. Adipocyte-specific deletion of Ip6k1 reduces diet-induced obesity by enhancing AMPK-mediated thermogenesis. *J Clin Invest* 2016;**126**:4273–4288.
24. Sun D, Li S, Wu H, Zhang M, Zhang X, Wei L, Qin X, Gao E. Oncostatin M (OSM) protects against cardiac ischaemia/reperfusion injury in diabetic mice by regulating apoptosis, mitochondrial biogenesis and insulin sensitivity. *J Cell Mol Med* 2015;**19**:1296–1307.
25. Mukherjee S, Chakraborty M, Ulmasov B, McCommis K, Zhang J, Carpenter D, Msengi EN, Haubner J, Guo C, Pike DP, Ghoshal S, Ford DA, Neuschwander-Tetri BA, Chakraborty A. Pleiotropic actions of IP6K1 mediate hepatic metabolic dysfunction to promote nonalcoholic fatty liver disease and steatohepatitis. *Mol Metab* 2021;**54**:101364.
26. Moritoh Y, Abe SI, Akiyama H, Kobayashi A, Koyama R, Hara R, Kasai S, Watanabe M. The enzymatic activity of inositol hexakisphosphate kinase controls circulating phosphate in mammals. *Nat Commun* 2021;**12**:4847.
27. Meyer RE, Fish RE. A review of tribromoethanol anesthesia for production of genetically engineered mice and rats. *Lab Anim (NY)* 2005;**34**:47–52.
28. Riley AM, Wang H, Shears SB, Potter BVL. Synthesis of an alpha-phosphono-alpha, alpha-difluoroacetamide analogue of the diphosphoinositol pentakisphosphate 5-InsP₇. *MedChemComm* 2019;**10**:1165–1172.
29. Wu M, Dul BE, Trevisan AJ, Fiedler D. Synthesis and characterization of non-hydrolysable diphosphoinositol polyphosphate second messengers. *Chem Sci* 2013;**4**:405–410.
30. Capolicchio S, Thakor DT, Linden A, Jessen HJ. Synthesis of unsymmetric diphospho-inositol polyphosphates. *Angewandte Chemie* 2013;**52**:6912–6916.
31. Furkert D, Hostachy S, Nadler-Holly M, Fiedler D. Triple affinity reagents to sample the mammalian inositol pyrophosphate interactome. *Cell Chem Biol* 2020;**27**:1097–1108 e1094.
32. Cai J, Chen X, Liu X, Li Z, Shi A, Tang X, Xia P, Zhang J, Yu P. AMPK: the key to ischemia-reperfusion injury. *J Cell Physiol* 2022;**237**:4079–4096.
33. Gu C, Liu J, Liu X, Zhang H, Luo J, Wang H, Locasale JW, Shears SB. Metabolic supervision by PPIP5K, an inositol pyrophosphate kinase/phosphatase, controls proliferation of the HCT116 tumor cell line. *Proc Natl Acad Sci USA* 2021;**118**:e2020187118.
34. Wang Y, Lau WB, Gao E, Tao L, Yuan Y, Li R, Wang X, Koch WJ, Ma XL. Cardiomyocyte-derived adiponectin is biologically active in protecting against myocardial ischemia-reperfusion injury. *Am J Physiol Endocrinol Metab* 2010;**298**:E663–E670.
35. Padmanabhan U, Dollins DE, Fridy PC, York JD, Downes CP. Characterization of a selective inhibitor of inositol hexakisphosphate kinases: use in defining biological roles and metabolic relationships of inositol pyrophosphates. *J Biol Chem* 2009;**284**:10571–10582.
36. Hostachy S, Utesch T, Franke K, Dornan GL, Furkert D, Türkaydin B, Hauke V, Sun H, Fiedler D. Dissecting the activation of insulin degrading enzyme by inositol pyrophosphates and their bisphosphonate analogs. *Chem Sci* 2021;**12**:10696–10702.
37. Liu M, Chen H, Wei L, Hu D, Dong K, Jia W, Dong LQ, Liu F. Endoplasmic reticulum (ER) localization is critical for DsbA-L protein to suppress ER stress and adiponectin downregulation in adipocytes. *J Biol Chem* 2015;**290**:10143–10148.
38. Combs TP, Pajvani UB, Berg AH, Lin Y, Jelicks LA, Laplante M, Nawrocki AR, Rajala MW, Parlow AF, Cheeseboro L, Ding YY, Russell RG, Lindemann D, Hartley A, Baker GR, Obici S, Deshaies Y, Ludgate M, Rossetti L, Scherer PE. A transgenic mouse with a deletion in the collagenous domain of adiponectin displays elevated circulating adiponectin and improved insulin sensitivity. *Endocrinology* 2004;**145**:367–383.
39. Zhou L, Liu F. Autophagy: roles in obesity-induced ER stress and adiponectin downregulation in adipocytes. *Autophagy* 2010;**6**:1196–1197.
40. Gavrilu A, Peng CK, Chan JL, Miettus JE, Goldberger AL, Mantzoros CS. Diurnal and ultradian dynamics of serum adiponectin in healthy men: comparison with leptin, circulating soluble leptin receptor, and cortisol patterns. *J Clin Endocrinol Metab* 2003;**88**:2838–2843.

41. Gómez-Abellan P, Gómez-Santos C, Madrid JA, Milagro FI, Campion J, Martínez JA, Ordóñez JM, Garaulet M. Circadian expression of adiponectin and its receptors in human adipose tissue. *Endocrinology* 2010;**151**:115–122.
42. Fu C, Rojas T, Chin AC, Cheng W, Bernstein IA, Albacarys LK, Wright WW, Snyder SH. Multiple aspects of male germ cell development and interactions with Sertoli cells require inositol hexakisphosphate kinase-1. *Sci Rep* 2018;**8**:7039.
43. Malla AB, Bhandari R. IP6K1 is essential for chromatoid body formation and temporal regulation of Tnp2 and Prm2 expression in mouse spermatids. *J Cell Sci* 2017;**130**:2854–2866.
44. Barbe A, Bongrani A, Mellouk N, Estienne A, Kurowska P, Grandhay J, Elfassy Y, Levy R, Rak A, Froment P, Dupont J. Mechanisms of adiponectin action in fertility: an overview from gametogenesis to gestation in humans and animal models in normal and pathological conditions. *Int J Mol Sci* 2019;**20**:1526.
45. Lee S, Kim MG, Ahn H, Kim S. Inositol pyrophosphates: signaling molecules with pleiotropic actions in mammals. *Molecules* 2020;**25**:2208.
46. Wang Z, Dou X, Gu D, Shen C, Yao T, Nguyen V, Braunschweig C, Song Z. 4-Hydroxynonenol differentially regulates adiponectin gene expression and secretion via activating PPARgamma and accelerating ubiquitin-proteasome degradation. *Mol Cell Endocrinol* 2012;**349**:222–231.
47. Gu D, Wang Z, Dou X, Zhang X, Li S, Vu L, Yao T, Song Z. Inhibition of ERK1/2 pathway suppresses adiponectin secretion via accelerating protein degradation by ubiquitin-proteasome system: relevance to obesity-related adiponectin decline. *Metab Clin Exp* 2013;**62**:1137–1148.
48. Aye I, Rosario FJ, Kramer A, Kristiansen O, Michelsen TM, Powell TL, Jansson T. Insulin increases adipose adiponectin in pregnancy by inhibiting ubiquitination and degradation: impact of obesity. *J Clin Endocrinol Metab* 2022;**107**:53–66.
49. Hampe L, Radjainia M, Xu C, Harris PWR, Bashiri G, Goldstone DC, Brimble MA, Wang Y, Mitra AK. Regulation and quality control of adiponectin assembly by endoplasmic reticulum chaperone ERp44. *J Biol Chem* 2015;**290**:18111–18123.
50. Hampe L, Xu C, Harris PWR, Chen J, Liu M, Middleditch M, Radjainia M, Wang Y, Mitra AK. Synthetic peptides designed to modulate adiponectin assembly improve obesity-related metabolic disorders. *Br J Pharmacol* 2017;**174**:4478–4492.
51. Vavassori S, Cortini M, Masui S, Sannino S, Anelli T, Caserta IR, Fagioli C, Mossuto MF, Fornili A, van Anken E, Degano M, Inaba K, Sitia R. A pH-regulated quality control cycle for surveillance of secretory protein assembly. *Mol Cell* 2013;**50**:783–792.
52. Li X, Zhang D, Vatner DF, Goedeke L, Hirabara SM, Zhang Y, Perry RJ, Shulman GI. Mechanisms by which adiponectin reverses high fat diet-induced insulin resistance in mice. *Proc Natl Acad Sci USA* 2020;**117**:32584–32593.
53. Shears SB. Intimate connections: inositol pyrophosphates at the interface of metabolic regulation and cell signaling. *J Cell Physiol* 2018;**233**:1897–1912.
54. Shears SB. Diphosphoinositol polyphosphates: metabolic messengers? *Mol Pharmacol* 2009;**76**:236–252.
55. Gokhale NA, Zaremba A, Janoshazi AK, Weaver JD, Shears SB. PIP5K1 modulates ligand competition between diphosphoinositol polyphosphates and PtdIns(3,4,5)P3 for polyphosphoinositide-binding domains. *Biochem J* 2013;**453**:413–426.
56. Dilworth L, Stennett D, Omoruyi F. Cellular and molecular activities of IP6 in disease prevention and therapy. *Biomolecules* 2023;**13**:972.
57. Amin RH, Mathews ST, Alli A, Leff T. Endogenously produced adiponectin protects cardiomyocytes from hypertrophy by a PPARgamma-dependent autocrine mechanism. *Am J Physiol Heart Circ Physiol* 2010;**299**:H690–H698.
58. Skurk C, Wittchen F, Suckau L, Witt H, Noutsias M, Fechner H, Schultheiss HP, Poller W. Description of a local cardiac adiponectin system and its deregulation in dilated cardiomyopathy. *Eur Heart J* 2008;**29**:1168–1180.
59. Solarewicz J, Manly A, Kokoszka S, Sleiman N, Leff T, Cala S. Adiponectin secretion from cardiomyocytes produces canonical multimers and partial co-localization with calsequestrin in junctional SR. *Mol Cell Biochem* 2019;**457**:201–214.
60. Tao L, Gao E, Jiao X, Yuan Y, Li S, Christopher TA, Lopez BL, Koch W, Chan L, Goldstein BJ, Ma XL. Adiponectin cardioprotection after myocardial ischemia/reperfusion involves the reduction of oxidative/nitrative stress. *Circulation* 2007;**115**:1408–1416.
61. Li N, Zhao S, Zhang Z, Zhu Y, Gliniak CM, Vishvanath L, An YA, Wang MY, Deng Y, Zhu Q, Shan B, Sherwood A, Onodera T, Oz OK, Gordillo R, Gupta RK, Liu M, Horvath TL, Dixit VD, Scherer PE. Adiponectin preserves metabolic fitness during aging. *eLife* 2021;**10**:e65108.
62. Jang AY, Scherer PE, Kim JY, Lim S, Koh KK. Adiponectin and cardiometabolic trait and mortality: where do we go? *Cardiovasc Res* 2022;**118**:2074–2084.
63. Cohen KE, Katunaric B, SenthilKumar G, McIntosh JJ, Freed JK. Vascular endothelial adiponectin signaling across the life span. *Am J Physiol Heart Circ Physiol* 2022;**322**:H57–H65.
64. Combs TP, Berg AH, Rajala MW, Klebanov S, Iyengar P, Jimenez-Chillaron JC, Patti ME, Klein SL, Weinstein RS, Scherer PE. Sexual differentiation, pregnancy, calorie restriction, and aging affect the adipocyte-specific secretory protein adiponectin. *Diabetes* 2003;**52**:268–276.
65. Chanduri M, Rai A, Malla AB, Wu M, Fiedler D, Mallik R, Bhandari R. Inositol hexakisphosphate kinase 1 (IP6K1) activity is required for cytoplasmic dynein-driven transport. *Biochem J* 2016;**473**:3031–3047.
66. Fleischer B, Xie J, Mayrleitner M, Shears SB, Palmer DJ, Fleischer S. Golgi coatamer binds, and forms K(+)-selective channels gated by, inositol polyphosphates. *J Biol Chem* 1994;**269**:17826–17832.
67. Chi H, Yang X, Kingsley PD, O'Keefe RJ, Puzas JE, Rosier RN, Shears SB, Reynolds PR. Targeted deletion of Minpp1 provides new insight into the activity of multiple inositol polyphosphate phosphatase in vivo. *Mol Cell Biol* 2000;**20**:6496–6507.
68. Windhorst S, Lin H, Blechner C, Fanick VW, Brandt L, Brehm MA, Mayr GW. Tumour cells can employ extracellular Ins(1,2,3,4,5,6)P(6) and multiple inositol-polyphosphate phosphatase 1 (MINPP1) dephosphorylation to improve their proliferation. *Biochem J* 2013;**450**:115–125.
69. Zubair M, Hamzah R, Griffin R, Ali N. Identification and functional characterization of multiple inositol polyphosphate phosphatase 1 (Minpp1) isoform-2 in exosomes with potential to modulate tumor microenvironment. *PLoS one* 2022;**17**:e0264451.
70. Kilari RS, Weaver JD, Shears SB, Safrany ST. Understanding inositol pyrophosphate metabolism and function: kinetic characterization of the DIPPs. *FEBS Lett* 2013;**587**:3464–3470.
71. Kilaparty SP, Singh A, Baltosser WH, Ali N. Computational analysis reveals a successive adaptation of multiple inositol polyphosphate phosphatase 1 in higher organisms through evolution. *Evol Bioinform Online* 2014;**10**:239–250.
72. Arita Y, Kihara S, Ouchi N, Takahashi M, Maeda K, Miyagawa J, Hotta K, Shimomura I, Nakamura T, Miyaoka K, Kuriyama H, Nishida M, Yamashita S, Okubo K, Matsubara K, Muraguchi M, Ohmoto Y, Funahashi T, Matsuzawa Y. Paradoxical decrease of an adipose-specific protein, adiponectin, in obesity. *Biochem Biophys Res Commun* 1999;**257**:79–83.
73. Chakraborty A, Koldobskiy MA, Bello NT, Maxwell M, Potter JJ, Juluri KR, Maag D, Kim S, Huang AS, Dailey MJ, Saleh M, Snowman AM, Moran TH, Mezey E, Snyder SH. Inositol pyrophosphates inhibit Akt signaling, thereby regulating insulin sensitivity and weight gain. *Cell* 2010;**143**:897–910.
74. Rounge TB, Page CM, Lepistö M, Ellonen P, Andreassen BK, Weiderpass E. Genome-wide DNA methylation in saliva and body size of adolescent girls. *Epigenomics* 2016;**8**:1495–1505.
75. Barclay RD, Beals JW, Drnevich J, Imai BS, Yau PM, Ulanov AV, Tillin NA, Villegas-Montes M, Paluska SA, Watt PW, De Lisio M, Burd NA, Mackenzie RW. Ingestion of lean meat elevates muscle inositol hexakisphosphate kinase 1 protein content independent of a distinct postprandial circulating proteome in young adults with obesity. *Metab Clin Exp* 2020;**102**:153996.

Translational perspective

Adiponectin is an adipocyte-derived circulating protein that protects cardiomyocytes from ischaemic injury. The high basal level and rapid elimination rate of adiponectin make exogenous administration challenging. Using global and tissue-specific *IP6K1* knockout animals, this study elucidates depleting 5-InsP₇ by genetic deletion or pharmacological inhibition of IP6K1 boosts plasma adiponectin, alleviating myocardial ischaemia–reperfusion injury. Mechanistically, we demonstrate that IP6K1 via its product 5-InsP₇ stabilizes adiponectin/Erp44 and DsbA-L/Ero1- α interactions, driving adiponectin intracellular degradation, which is responsible for up to 50% of futile intracellular loss of adiponectin. Our study may provide novel strategies for cardioprotection by elevating plasma adiponectin.